NOAA Technical Memorandum ERL ARL-36

U.S. DEPARTMENT OF COMMERCE
NATIONAL OCEANIC AND ATMOSPHERIC ADMINISTRATION
Environmental Research Laboratories

Transport, Deposition, and Meteorological Studies of Nuclear Debris in the Atmosphere

ROBERT J. LIST, Editor

Annual Progress Report
July 1970 - June 1971
to the Division of Biology and Medicine
U.S. Atomic Energy Commission

Air Resources
Laboratories
SILVER SPRING,
MARYLAND
March 1972

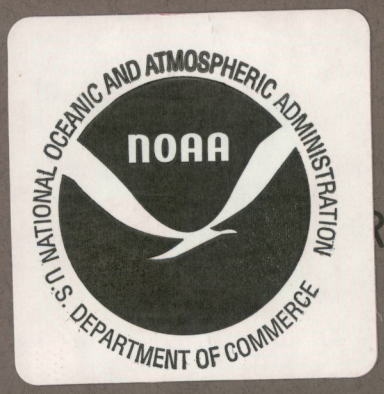

RONMENTAL RESEARCH LABORATORIES

AIR RESOURCES LABORATORIES

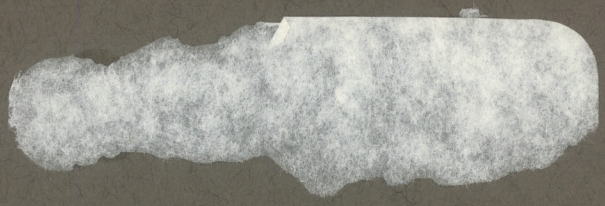

IMPORTANT NOTICE

Technical Memoranda are used to insure prompt dissemination of special studies which, though of interest to the scientific community, may not be ready for formal publication. Since these papers may later be published in a modified form to include more recent information or research results, abstracting, citing, or reproducing this paper in the open literature is not encouraged. Contact the author for additional information on the subject matter discussed in this Memorandum.

NATIONAL OCEANIC AND ATMOSPHERIC ADMINISTRATION

U.S. DEPARTMENT OF COMMERCE
National Oceanic and Atmospheric Administration
Environmental Research Laboratories

NOAA Technical Memorandum ERL ARL-36

Air Resources Laboratories.

TRANSPORT, DEPOSITION, AND METEOROLOGICAL STUDIES OF NUCLEAR DEBRIS IN THE ATMOSPHERE

Robert J. List, Editor

Contributors

Thomas E. Ashenfelter
Gilbert J. Ferber
Jerome L. Heffter
Lester Machta
Albion D. Taylor
Kosta Telegadas

Annual Progress Report
July 1970 - June 1971
to the Division of Biology and Medicine
U.S. Atomic Energy Commission

Air Resources Laboratories
Silver Spring, Maryland
March 1972

TABLE OF CONTENTS

TRANSPORT, DEPOSITION, AND METEOROLOGICAL STUDIES OF NUCLEAR DEBRIS IN THE ATMOSPHERE

1. INTRODUCTION

Robert J. List, Editor

The close working relationship between the Atomic Energy Commission (AEC) and the National Oceanic and Atmospheric Administration (NOAA) had its beginnings with the establishment of the AEC and with early nuclear weapons test operations. There were three areas of interaction. In 1948 the Weather Bureau (now the NOAA National Weather Service) began providing meteorological services required in connection with the establishment and operation of the Oak Ridge, Tennessee, production and research facilities. This group, which is now supported in part by the AEC Division of Biology and Medicine (DBM) and in part by NOAA, has evolved into a leading center of operational and theoretical research into meteorological problems relating to the use of nuclear energy. Another group, headquartered in Washington, provided meteorological studies and consultation in connection with the siting of new AEC production facilities and power reactors and the meteorological operations and research required by the National Reactor Testing Station near Idaho Falls, Idaho. This group is supported by the AEC Divisions of Reactor Development and Technology and Reactor Licensing. Both groups are now components of the NOAA Air Resources Laboratories (ARL).

The third area of interaction began with a group of theoretical and operational meteorologists assembled in 1948 to investigate the long-range atmospheric transport of nuclear debris. Dr. Lester Machta, now Director of the Air Resources Laboratories, was in charge of this group. The success of their early activities led to a much broader participation in

many other aspects of nuclear testing and nuclear technology. The third group, now called the Air Resources Radioactivity Laboratory (ARRL), a component of the Air Resources Laboratories, has provided expertise and continuity in fallout studies over the past two decades and also has made major contributions in the use of radioactive isotopes for investigating atmospheric processes. A major portion of its work has been supported by the AEC for more than two decades. The work of ARRL for the Division of Biology and Medicine, Fallout Studies Branch, for Fiscal Year 1971 under Contract AT(49-7)-4 is reported here.

2. LOCAL FALLOUT PREDICTION
(G. J. Ferber)

ARRL has long provided the AEC with fallout prediction capability involving the development, verification, and operational use of models and techniques for predicting dose-rate levels and accumulated dose caused by local fallout of radioactive debris. Personnel have been assigned to the AEC Test Manager's Fallout Prediction Unit for all U.S. atmospheric nuclear test series since 1956. The combined experience of the present ARRL staff includes operational fallout prediction at the Redwing (1956), Plumbbob (1957), Hardtack I and II (1958) and Dominic I and II (1962) nuclear tests in Nevada and the Pacific. These tests involved surface, air and underground bursts, as well as many detonations atop towers and on balloons.

The ARL computerized fallout prediction model is a modification of the manual prediction technique used for operational pre-shot predictions for U.S. nuclear tests from 1955 to the end of above-ground testing in 1962. Development of the prediction method was begun in 1954 (Nagler et al., 1955), and there has been a continuing effort to improve the model using meteorological and fallout data from nuclear tests in Nevada and the Pacific. The model uses initial distributions of radioactivity, as a function of particle size and height in a stabilized nuclear cloud, as derived from measured fallout deposition patterns. Radioactivity distributions were initially developed for nuclear detonations atop towers and for air-bursts. More recently, distributions have been derived for surface bursts and for cratering detonations.

A computerized version of the model (Fleshel and Seery, 1968) was developed specifically to aid in evaluating the feasibility of nuclear excavation of a sea-level canal (Ferber and Palmer, 1970). The computer program was designed to

provide individual fallout patterns or composite maps of total fallout from multiple bursts, and also to compute fallout fields for a large number of different wind soundings and produce statistics on the frequency of occurrence of any specified dose levels. As in most computer fallout models, the nuclear cloud is subdivided into a number of horizontal slices, and fallout particles in each slice are grouped into discrete size ranges. Each particle size range from each cloud slice is treated as a disk which is transported by winds as it falls to the ground by gravitational settling. The transport calculation requires measurements or forecasts of winds at altitudes from the ground to the top of the nuclear cloud. In this model, transport calculations are based on a single wind sounding; i.e., winds vary with altitude, but the wind in each horizontal layer of the atmosphere is assumed to remain constant during fallout deposition. The principal advantage of this computer program lies in the use of a technique that determines the ground position of all particles in the cloud from a "fallout hodograph" computed for a single particle. This eliminates the need to calculate a trajectory for each falling particle and thus increases the computational speed. A unique method for determining the grid points covered by a landed disk also contributes to the unusually fast computational speed achieved with this program. The time required to calculate a fallout pattern for a single nuclear burst is less than 10 sec on a CDC-6600 or comparable computer. Such a high speed makes it economically feasible to perform detailed statistical studies of fallout for a proposed nuclear event. For example, wind soundings for a month, or a year, could be loaded into the computer and a fallout pattern calculated for each sounding. The statistics module could then be used to provide a map showing the frequency with which any specified dose levels are exceeded at each

grid point. Fallout statistics based on a full year of daily wind soundings would require about an hour of computer time.

Current work includes (1) analysis of fallout from recent cratering detonations to provide information on the amount and distribution of radioactivity in the initial nuclear cloud from this type of event, and (2) computer program modifications to increase accuracy and efficiency and to adapt it more readily to use in possible future nuclear test operations or Plowshare events. When the program modifications are completed, a report will be prepared documenting the fallout model and describing its modes of operation and uses in fallout prediction. It will be followed by a report on the verification of model predictions against actual fallout patterns resulting from the various types of nuclear detonations (air, tower, surface, and underground bursts). In effect, the computer program and companion reports are intended to summarize our experience in operational prediction of local fallout and provide a prediction capability for any future nuclear test operations or Plowshare applications. Work completed in FY 71 is summarized below.

2.1 Fallout Model for Cratering Events

An improved fallout prediction model is needed for planning and conducting nuclear cratering experiments and, eventually, for Plowshare applications of cratering technology. At present, very conservative assumptions must be used because of limited experience with fallout from cratering detonations. As a result, safety evaluations for a proposed event may be overly cautious, operational restrictions may be severe, and more people may be evacuated prior to an event than actually required. Improvement in prediction capability will allow more realistic pre-shot evaluations and operational controls, thus aiding the advancement of nuclear excavation technology.

2.1.1 Radioactivity Distribution in Nuclear Cloud

The radioactivity distribution presently used in the model for cratering events is actually based on measured hourly fallout deposition rates from near-surface detonations (Johnnie-Boy and Smallboy) and subjectively modified for cratering detonations. Fallout deposition rates have now been calculated from the measured downwind distribution of fallout from several U.S. nuclear cratering experiments. A complete analysis of the fallout deposition pattern produced by the most recent cratering detonation (Schooner) is now available from ARL-Las Vegas and hourly deposition rates will also be determined for this shot. Results for all cratering events to date will then be used to revise the radioactivity distribution in the cratering fallout model.

The method used to obtain radioactivity distributions in the initial nuclear cloud from fallout deposition patterns will be briefly described here, along with results obtained thus far. The downwind distribution of fallout is affected primarily by (1) the height of the nuclear cloud, (2) the initial distribution of radioactivity with particle size and height, and (3) the wind field through which the particles fall. Most of the complicating effects of differing wind fields for each detonation can be eliminated by confining our attention to the fraction of local fallout deposited each hour, a quantity that is independent of the winds (assuming that vertical wind velocities are small compared to particle settling rates). In practice, results are not completely independent of existing wind conditions, since measurements of fallout time-of-arrival are generally not available throughout the fallout patterns, and observed winds must be used to help determine the isochrones of fallout arrival. By integrating the fallout pattern (R/hr-miles^2) between hourly isochrones, the fraction of local fallout deposited per hour can

be determined. (Note that fractions are used rather than actual amounts deposited since the total amount of fallout for any detonation is dependent on the height, or depth, of burst, fission yield, induced activities and other factors.) The limits of integration also may be adjusted to eliminate cloud height effects. In our analysis, all time-of-arrival isochrones have been adjusted to those for a cloud top at 12,000 ft above the ground. This is accomplished by assuming, as a reasonable approximation, that, for any particle-size range from any altitude in the nuclear cloud, time of arrival at the ground is proportional to the cloud top altitude. Consider, for example, a fallout pattern resulting from a cloud that rose to 6000 ft. Fallout deposited during the first half-hour after detonation would have taken twice as long to fall from a 12,000-ft cloud and, thus, would have been deposited during the first hour. Similarly, activity deposited between one-half hour and 1 hr would have been deposited between 1 and 2 hrs from a 12,000-ft cloud. In this way, fallout arrival isochrones are relabelled to normalize all fallout patterns to a 12,000-ft cloud top and then hourly deposition amounts are determined. Some results are presented in table 2.1 and figure 2.1 as percent of local fallout deposited per hour (normalized) for several near-surface and underground cratering detonations. Deposition rates are remarkably similar for all these detonations with surprisingly little difference between the near-surface (Smallboy, Johnnie-Boy) and deeply buried shots. Deposition from near-surface detonations appears to be only slightly lower in the first hour and somewhat higher in the next two hours when compared to underground detonations. Note that deposition rates for Buggy appear to be anomalously low from 1 to 5 hrs after detonation. This may be real or it may be caused by a large percentage uncertainty in the estimated cloud top (3000 ft) used to adjust arrival times to those for a 12,000-ft cloud.

*Table 2.1. Percent of Total Local Fallout Deposited Each Hour**

	Detonation						
	Small Boy	Johnnie Boy	ESS	Sedan	Danny Boy	Buggy	Tower Model
	Scaled Depth**						
	-8	2	63	164	141	131	--
Hours	Percent Deposited						
0-1	80.	81.	83.	84.	86.	88.	64.
1-2	9.7	8.8	6.0	6.6	6.8	4.8	20.
2-3	4.2	4.7	4.2	3.6	3.7	2.5	8.7
3-4	2.2	2.4	2.3	2.1	2.0	1.3	4.4
4-5	1.6	1.2	1.5	1.0	1.4	0.80	2.5
5-6	1.0	0.92	1.1	0.75	1.0	0.76	--
6-7	0.65	0.63	0.73	0.70	--	0.62	--
7-8	0.43	--	0.44	0.65	--	0.57	--
8-9	0.30	--	0.37	0.63	--	0.44	--
9-10	--	--	0.20	--	--	0.21	--
10-11	--	--	0.13	--	--	--	--
11-12	--	--	0.12	--	--	--	--
12-13	--	--	0.09	--	--	--	--

* Normalized to 12,000 ft cloud top.
**Scaled depth = $D/\gamma 0.294$ where D is depth of burial in feet and Y is yield in kilotons.

Also shown for comparison (table 2.1 and fig. 2.1) are hourly deposition rates used in the ARL model for detonations atop towers. This model distribution, obtained by averaging results from many tower shots at the Nevada Test Site, is distinctly different from the surface and underground fallout distributions.

Results thus far are very encouraging from the standpoint of fallout prediction for cratering detonations. In spite of the range of conditions represented by these detonations (e.g., differences in type of nuclear device, depth of burial, type of rock, water content, etc.) that influence the total amount of fallout and its radiochemical composition, it appears that the rate of deposition of gross gamma activity remains fairly constant. After analysis of Schooner fallout is completed, the radioactivity distribution currently used (also shown in

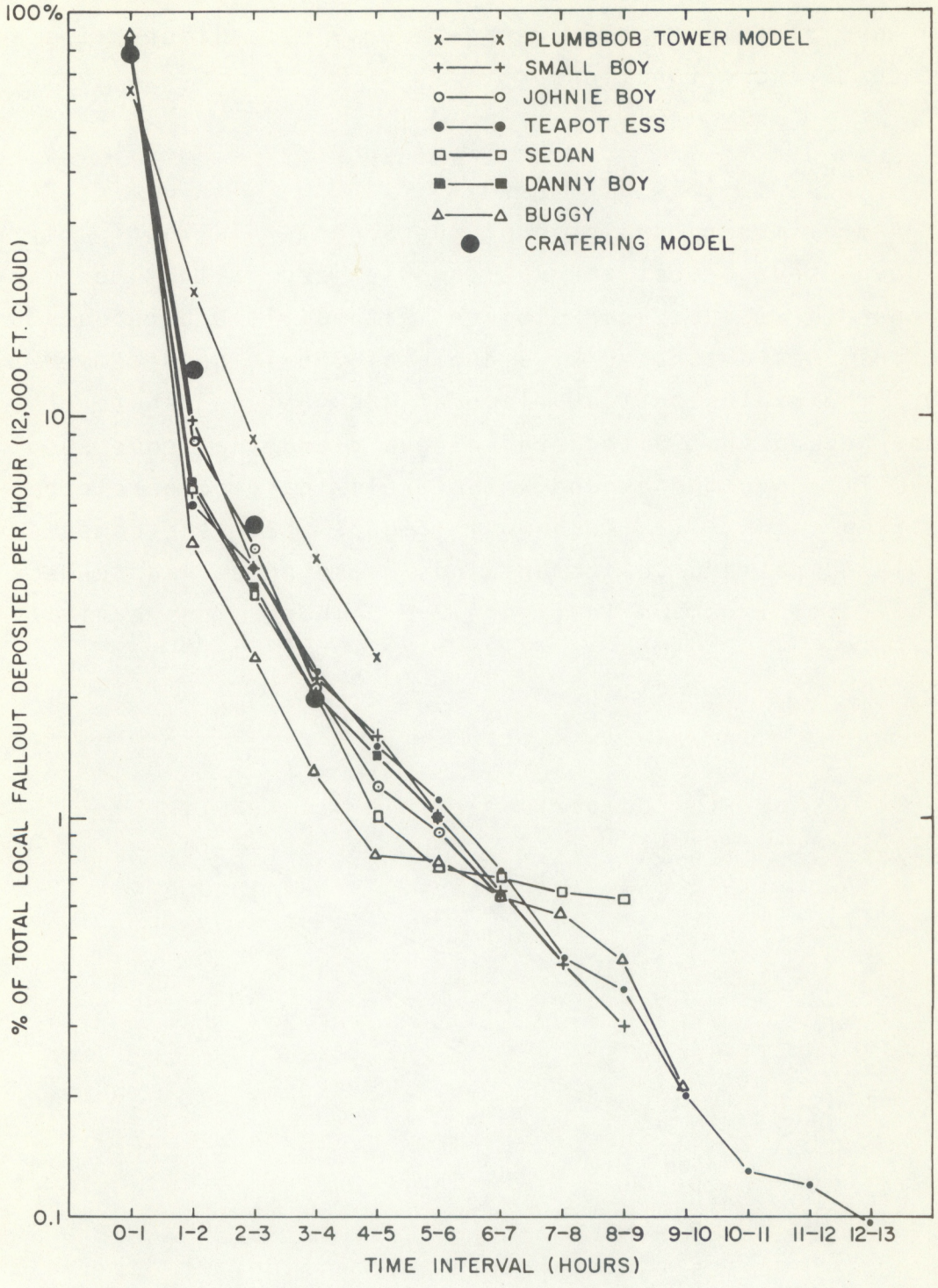

Figure 2.1. Comparison of hourly fallout deposition rates (normalized to a 12,000 ft cloud).

fig. 2.1) in the ARL cratering model will be revised to conform more closely to the average hourly deposition rates from past cratering detonations.

2.1.2 Model Verification

A preliminary analysis of the Schooner fallout pattern has been used to test the ARL computerized fallout model. The Schooner thermonuclear explosive, with a yield of about 30 kilotons, was detonated at a depth of 355 ft on December 8, 1968. The explosion took place at 0800 PST on Pahute Mesa at the Nevada Test Site, producing a cloud that rose about 13,000 ft above the ground. The preliminary dose-rate pattern (R/hr at H + 1) is shown in figure 2.2. The computer-calculated pattern, based on winds measured on Pahute Mesa at shot-time is shown in figure 2.3. These winds exhibited

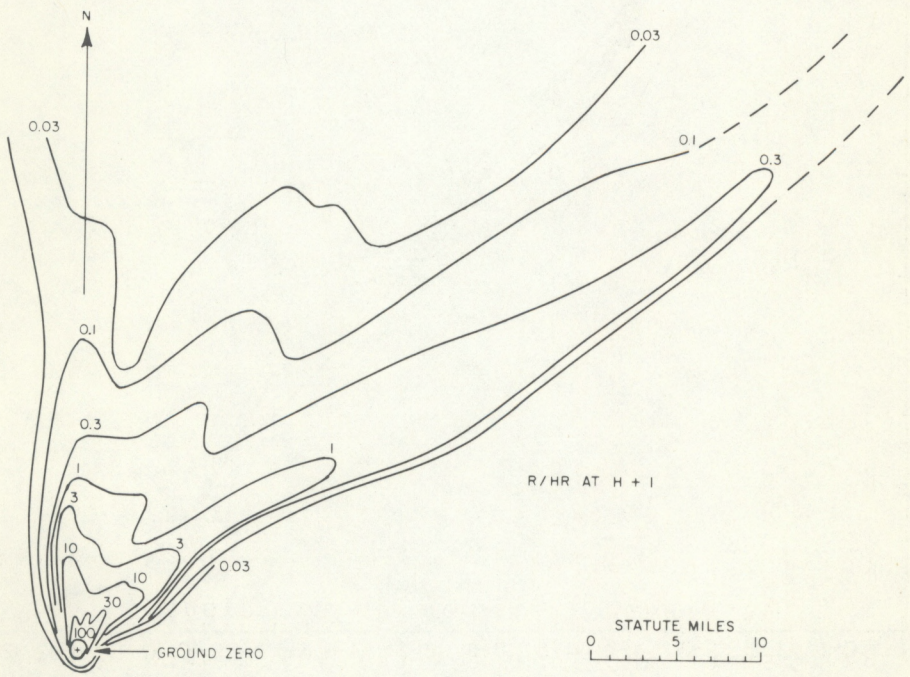

Figure 2.2. Preliminary analysis of Schooner local fallout pattern (R/hr at H + 1).

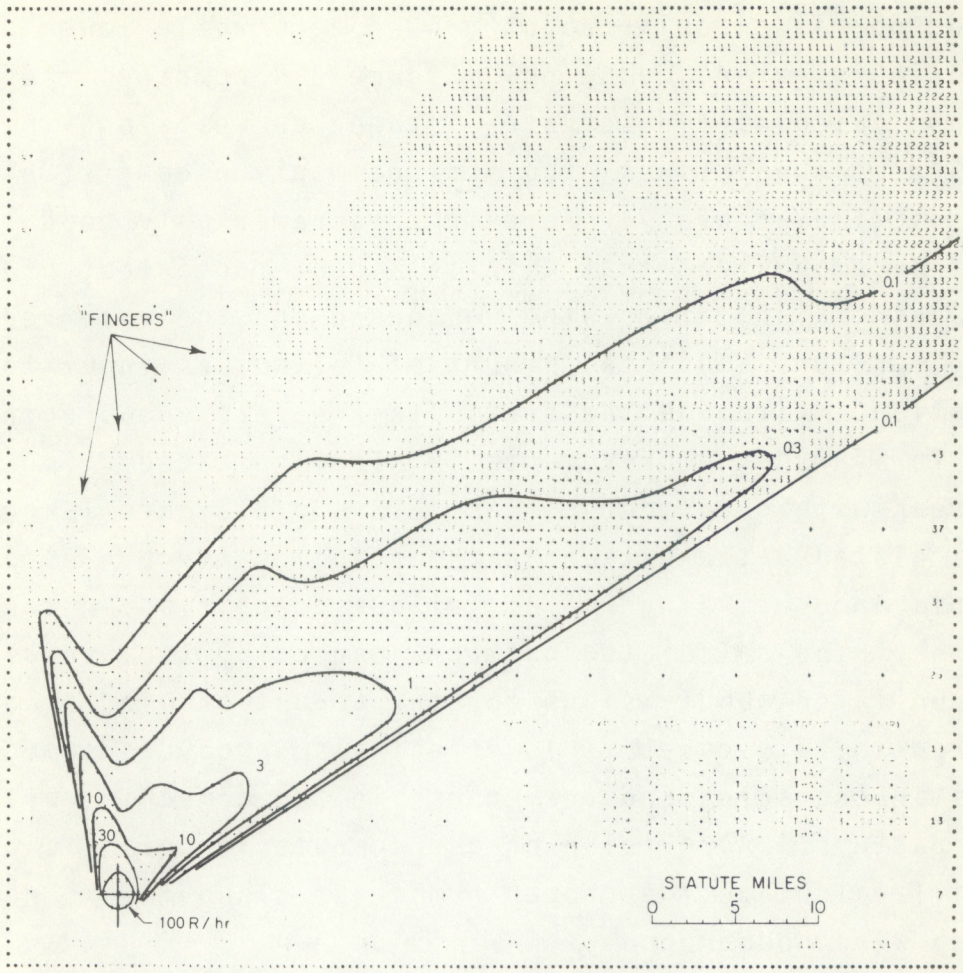

Figure 2.3. Computer-calculated fallout pattern for Schooner (R/hr at H + 1).

considerable directional shear with altitude, with the lower portion of the cloud (base surge) being carried toward the north-northwest and the upper portion toward the northeast. The actual fallout pattern shows the main "hot-line" toward the northeast and the base surge hot-line toward the north. A third hot-line, not as well-defined, may be attributed to fallout from the middle altitudes of the cloud. The calculated pattern shows the same general shape with the main hot line from the upper part of the cloud, a second well-defined hotline from the base surge and even a hint of the middle altitude hot line. Note also that in both patterns, the 100

R/hr contour is circular about ground zero while lower dose-rate contours extend downwind. Figure 2.4 compares the measured and calculated dose rate-distance curves along the base surge and main hot lines, the most commonly used test of fallout prediction accuracy. Agreement is remarkably good, but it must be emphasized that this is a post-facto test of the model, using a shot-time wind hodograph and the observed cloud dimensions and total amount of fallout as input to the calculation. Although these results are very encouraging, a need for further improvements is also indicated. For example, areas within contours (figs. 2.2 and 2.3) are larger in the calculated pattern than in the actual pattern. Also note the appearance of "fingers" of fallout deposition in the outer portions of the calculated pattern, caused by the use of too few cloud layer subdivisions for the amount of wind shear encountered in this case. This effect also produces some less obvious inaccuracies and unevenness in the close-in portion of the pattern. A revision of the computer program is planned that will calculate the proper number of cloud layers needed for each wind hodograph.

2.2 Computer Program Modifications

The fallout computer program has been modified for use with high-yield nuclear detonations. Fallout calculations can now be made for nuclear clouds extending up to an altitude of 150,000 ft (formerly limited to 60,000 ft); thus, the program would be suitable for use in any future resumption of Pacific nuclear tests.

Radioactive decay calculations are being revised to allow computation of deposition patterns for individual nuclides, as well as total gross gamma patterns. At present, only gross gamma decay following a t^{-n} law can be calculated, which often necessitates hand-computation and summation of

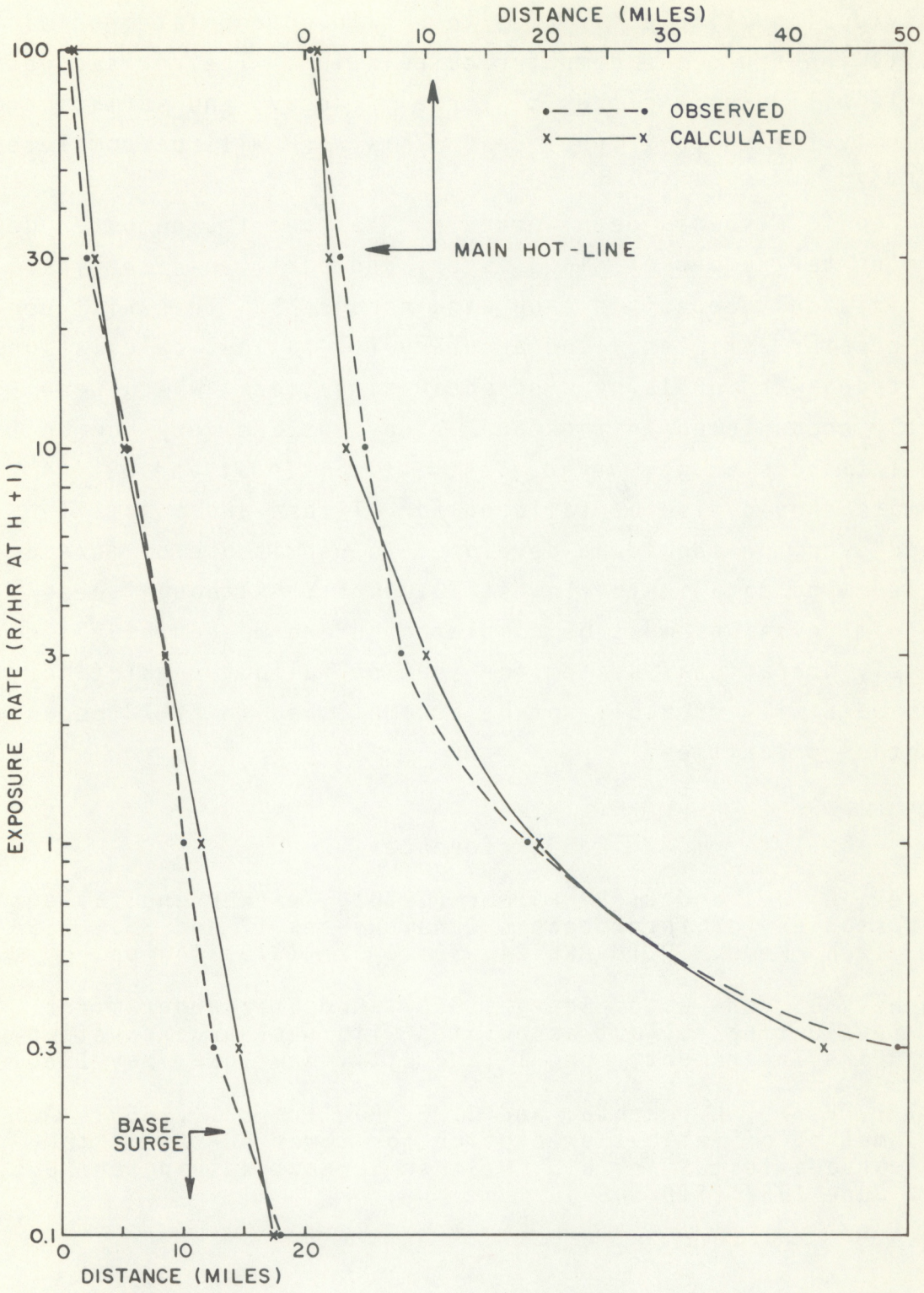

Figure 2.4. Calculated and observed Schooner hot-line exposure rates.

individual nuclide activities to obtain appropriate radioactivity inputs to the computer calculation. The revised decay module will permit either t^{-n} or $e^{-\lambda t}$ decay, and summation of activity for up to 12 nuclides. This work will be completed in FY 72.

Logic also has been worked out to have the computer determine the number of cloud layers and particle-size class subdivisions needed for each wind hodograph. This will permit greater efficiency and accuracy for fallout calculations in strong wind or large wind shear situations, which were rarely encountered in the canal study but are very common in mid-latitudes (e.g., Nevada Test Site). Input and output formats should also be tailored for NTS use and a "small cloud" version should be developed to permit use of more detailed wind data in the lowest 20,000 ft. Although these program revisions must be completed before we can have a completely operational system for routine fallout prediction, this work will probably not be accomplished in FY 72 because of other priorities.

2.3 References

Ferber, G. J., and T. R. Palmer (1970), Weather and fallout studies for Interoceanic Canal Routes 17 and 25. ESSA Tech. Memo, ERLTM-ARL-24, September 1970, 140 pp.

Fleshel, B., and C. J. Seery (1968), Computer program for evaluating fallout associated with nuclear excavation, Ford Instrument, Long Island City, New York, May 1968.

Nagler, K. M., L. Machta, and J. F. Pooler, Jr. (1955), A method of fallout prediction for tower bursts at the Nevada Test Site; U.S. Weather Bureau, Washington, D.C., June 1955 (TID 5489).

3. LONG-RANGE PLUME DIFFUSION

(G. J. Ferber, R. J. List, and A. D. Taylor)

Planning and feasibility studies were conducted in FY 71 for a concerted attack on problems of long-range transport and diffusion of continuous and detached plumes. This work included:

(a) an investigation of the feasibility of using sulphur hexafluoride (SF_6) as a gaseous tracer in a series of field experiments, culminating in cross-country sampling to study plume behaviour over distances up to 4000 km and travel times of several days, and

(b) the use of computer simulations to help plan these experiments and interpret results, with feedback of experimental results to improve computer predictions of long-range plume behavior.

3.1 Planning for Tracer Experiments

Plans were developed for a series of experiments in which SF_6 would be released at the ground or from stacks, over periods of 4-24 hrs, and extensive air sampling networks would be set up to determine the distribution of SF_6 as a function of time and distance from the source - both at ground level and aloft. The project goal is to improve our ability to predict transport, spread (horizontal and vertical), and dilution of plumes out to distances of several thousand kilometers from a source. Sampling data obtained in these experiments would be used to test existing air trajectory computation techniques and diffusion models and to develop improved models. Although this type of experiment is inherently difficult and costly, the use of SF_6 as a tracer appears to offer promise of success. It is relatively inexpensive, has no known harmful effects, and may therefore be released in large quantities. Sensitivity of existing detection techniques is sufficiently high (1 part in 10^{14}) to permit evaluation of

samples of the effluent collected across the United States over a period of several days. The major question with respect to feasibility of long-range detection concerns the magnitude of existing background concentrations of SF_6 in the atmosphere. A background sampling program will be conducted to resolve this question.

3.1.1 Feasibility of Long-Range Detection of SF_6

Sulphur hexafluoride has a higher dielectric constant than dry air and is used by industry as an insulator in electrical equipment, such as circuit breakers, capacitors, transformers, transmission lines and microwave components. It is also used in very large quantities as an insulator in particle accelerators. Toxic hydrofluoric acid may be present as an impurity (up to 0.2%) in bottled SF_6. The gas is colorless, odorless, tasteless, nonflammable, and non-toxic. A routine quality control procedure in the manufacture of SF_6 is to subject mice to an atmosphere of 80% SF_6 and 20% oxygen for 24 hrs without any visible effect. It is usually packaged as liquified gas in cylinders containing 115 lb of SF_6 and costs about $2.00 per lb.

Information on background concentrations has been gathered from the meager literature on the subject (Lovelock, 1971; Gatz and Carson, 1970; Turk et al., 1968) and from contacts with individuals and organizations involved in development of systems for release, sampling, detection, and analysis of SF_6. Indications are that background concentrations in the United States are always greater than 3×10^{-2} picoliters of SF_6 per liter of air (3 parts in 10^{14} by volume or 15 parts in 10^{14} by weight) and usually less than 2×10^{-1} p1/1; however, concentrations above 1 p1/1 have been found at times in and downwind of large urban areas. Values above 100 p1/1 have been obtained in the immediate vicinity of sources (power plants, accelerators).

The amount of SF_6 required for a cross-country experiment has been established on the optimistic assumption that a peak concentration of 2 p1/1 four days after release would be adequate to permit unambiguous definition of the plume. In a favorable meteorological setting, with strong, steady wind flow and relatively little wind shear,

$$Q = \chi_{p(96)} \sqrt{2\pi}\, \sigma_y\, L\, u, \qquad (3.1)$$

where Q is the release rate (lb/hr),

$\chi_{p(96)}$ is the desired peak concentration at 96 hrs (2 p1/1 or 2.2×10^{-11} lbs/m^3),

σ_y is the crosswind standard deviation of the plume at 96 hrs (assume 96 n miles or 1.78×10^5 m),

L is the mixing layer (assume 3×10^3 m),

u is the mean wind speed (assume 20 knots or 3.7×10^4 m/hr).

With these assumptions the required release rate, Q, is about 1100 lb/hr. If a 12-hr release is used to simulate a continuous plume, a total of about 6 tons of SF_6 would be needed. A release of this magnitude appears to be feasible although it may be approaching the upper limit from the standpoint of cost and manageability. Final judgement as to the feasibility of a cross-country experiment must await the results of an extensive background survey. The northeastern section of the country will be most critical, since plume concentrations will be low and SF_6 background concentrations are expected to be highest in this region. About 200 air samples will be collected at various locations throughout the United States to determine background concentrations and their variability.

Instrumentation and procedures have been developed for detection and quantitative analysis of SF_6 using gas chromatography (Clemons, et al., 1968). This technique permits rapid (minutes per sample) analysis of a large number of samples. Only 50 cc of sample is required for analysis. The limit of detection is 10^{-2} p1/1 for laboratory analysis involving preconcentration of the sample. Portable instruments are being developed which will provide real-time sample analysis with an expected detection limit of about 0.5 p1/1. Most field sampling would be done with evacuated flasks (perhaps fitted with a critical orifice to obtain time-averaged samples) which would be returned to the laboratory for analysis.

3.1.2 Preliminary Plan for Field Experiments

A proposed program of tracer experiments, contingent on favorable results in the background surveys, is outlined in table 3.1. This rather ambitious plan envisions about 20 experiments to be conducted over a period of several years. Table 3.2 summarizes estimates of amount and duration of each SF_6 release, and the total number of air samples to be collected and analyzed in each short-, medium-, and long-range experiment. Release amounts are based on the assumption that a peak centerline concentration of 2 p1/1 at the most distant sampling arc would be sufficient to distinguish the plume from background concentrations. In all, about 40 tons of SF_6, costing about $160,000, would be released. If this material eventually spreads uniformly throughout the atmosphere, the resulting increase in SF_6 background would be about 0.01 p1/1.

Several short-range experiments will be conducted, probably at the National Reactor Testing Station, Idaho Falls, primarily to test equipment and procedures for releasing, sampling, and analyzing SF_6. Fixed sampling stations and

Table 3.1. Proposed SF_6 Experiments

Type	Number
A. Background Survey	--
B. Short Range (70 km) Test equipment and techniques	3
C. Intermediate Range (500 km) Sample several arcs at ground level and aloft (aircraft) to measure horizontal and vertical distributions, and dilution factors to about 24 hrs after release.	6
D. Terrain Effects Studies 1. Hilly terrain and mountains 2. Trajectory over water (lake, ocean)	5
E. Long-Range (2000-4000 km) Sample at ground and aloft out to 3 or 4 days after release	6

mobile units (trucks or station wagons) would be deployed along several arcs at distances up to 70 km from the release point. Aircraft would also be used to take samples along and perpendicular to these arcs at several altitudes from about 100 m to about 2 km. Results would be used in the final design of intermediate-range experiments.

About six intermediate-range experiments (to about 500 km) will be conducted at different locations and under various meteorological conditions. Again, air sampling would be done along several arcs at the ground (using Interstate Highways) and at several altitudes aloft. Existing weather stations (surface and upper-air) would provide meteorological data, and some could also be used for air sampling.

We also plan to conduct several experiments designed to study the effects of terrain on effluent distribution immediately downwind and on long-range plume concentrations. Releases over hilly terrain could be carried out at the Nevada

Table 3.2. Proposed SF_6 Releases and Sample Collections

Experiment	Distance (km)	SF_6 Release		No. of Samples	
		Amount (tons)	Duration (hr)	Ground	Aloft
Short Range	70	0.1	4	100	100
Intermediate	500	1	8	300	200
Long Range	3000	6	12	1000	400

Test Site, Hanford Laboratory, or the Idaho Falls facility. Other experiments investigating the effects of over-water trajectories on plume behavior might be conducted over the Great Lakes or off the East Coast.

Since long-range effects are of primary interest, a long-range experiment may be attempted after one or two successful tries at intermediate range. Then a determination could be made as to where further efforts should be concentrated. Present plans call for about six long-range experiments with releases most likely from the Hanford Laboratory and the Nevada Test Site. Figure 3.1 shows possible sampling arcs and idealized plumes at 1, 2, and 3 days after a 24-hr release at Hanford. Sampling along the more distant arcs would be done primarily by aircraft, at altitudes from as low as 150 m to about 3 km. Actual flight paths and sampling intervals would be assigned on the basis of meteorological trajectory forecasts and plume positions determined from early *in-situ* sampling results. Air sampling at ground level also would be done at weather stations on several lines crossing the entire United States, as illustrated in figure 3.2.

A considerable meteorological effort will be required to forecast plume behavior over a period of three days or more to vector sampling aircraft through the plume and to determine optimum sampling times for ground stations. Constant-volume balloons (tetroons) set to float at predetermined

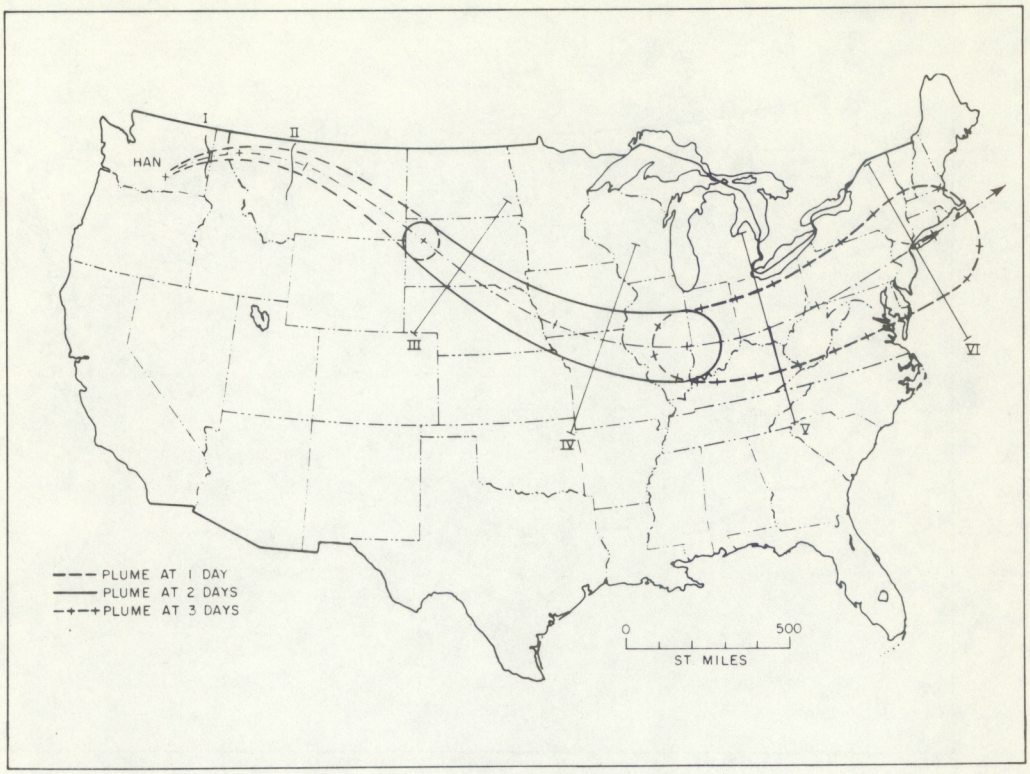

Figure 3.1. Idealized plume and sampling lines for a long-range experiment.

altitudes would be tracked by radar to aid in following the invisible plume. One purpose of this program is to evaluate the capability of post-facto analysis to determine the long-range history of a plume using only standard weather data from the existing upper-air networks. Detailed post-facto analysis using sampling data in conjunction with standard meteorological data and special observations (tetroon tracks, extra wind soundings, stability parameters, etc.) will also be done to understand the plume behavior in relation to meteorological conditions and to develop a model of long-range transport and diffusion processes.

It is anticipated that funding for this program in FY 72 and beyond will be provided by the Department of Defense, and no further AEC funding will be required.

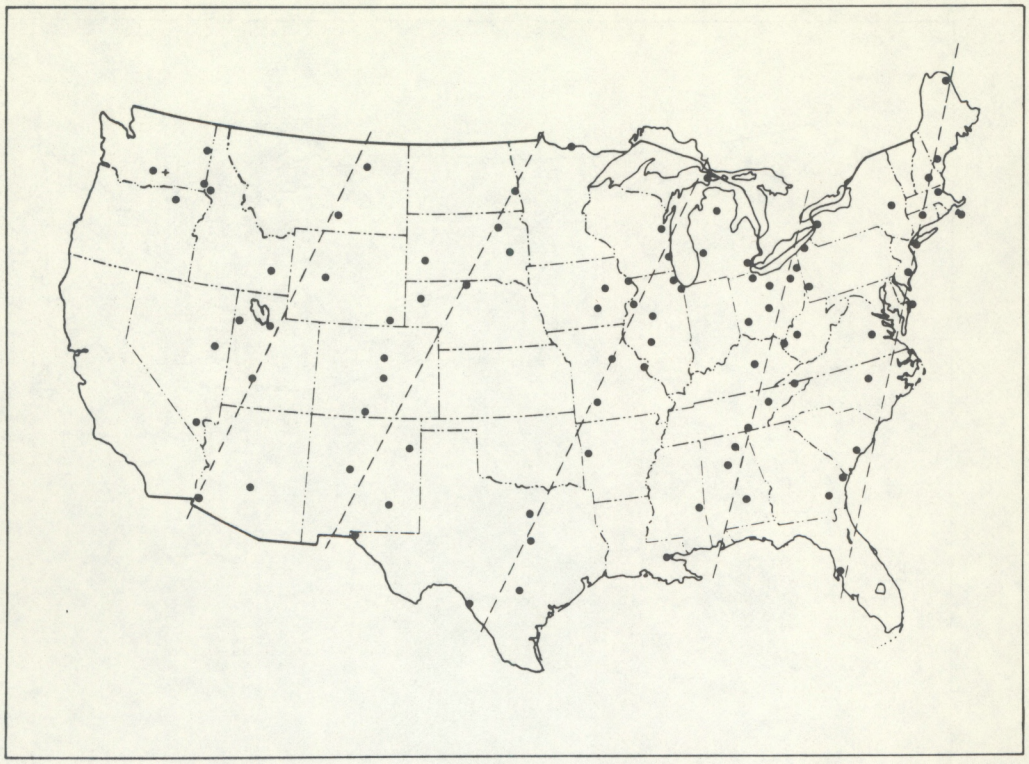

Figure 3.2. Selected weather station sites for additional sampling.

3.2 Computer Simulation

A computer model, which simulates transport and diffusion of plumes over a period of several days, is being developed for use in conjunction with field experiments. Computer calculations will be used to help design the experiments and interpret results. Field data will, in turn, be used to verify and improve model predictions. Also, the separate and combined effects of wind speed, shear, and diffusion parameters can best be studied by computer simulation.

Work has begun to adapt an existing computer model designated the "S^3 Urban Air Pollution Model." This model uses a 3-dimensional fixed grid in which a large number of discrete parcels, each representing a specified amount of pollutant, are advected by the wind field and dispersed in

accord with K-theory diffusion. Wind speeds and diffusion coefficients in the x, y, and z directions are completely variable, being specified at each grid point for each time step. Diffusion is included as a pseudo-velocity added to the advection velocity for each parcel. The average concentration of pollutant in each grid cell at each time step is determined by the number and position of parcels in the cell. This "parcel-in-cell" computing routine for modelling diffusion-advection problems is an outgrowth of research in fluid dynamics originally done at the AEC Los Alamos Laboratory. The adaption to diffusion-advection problems was performed by Sklarew (1970) at Science, Systems, and Software (S^3).

The chief advantage of the parcel-in-cell method over other finite difference schemes is that it eliminates the phenomenon of spurious diffusion due to the advection terms. To explain the cause of spurious diffusion, let us consider the effect of advection terms only on a single point mass. In a conventional procedure, values of concentration density are computed only for a finite number of grid points. A point mass would be represented by setting the concentration at one of these grid points to a positive value, the rest to zero. After one time step, the point mass (under advection only) usually would have moved to a location between grid points. In consequence, to represent the new situation, total mass is spread over two, or four, or more neighboring grid locations. Various rules would be observed, e.g., the center of mass of the spread-out representation must agree with the actual position of the point mass. A higher order scheme (generally more accurate if the fields are smooth) would require other moments to be conserved, which would require still more neighboring grid values to be non-zero.

In a conventional calculating scheme, these spread-out values are made permanent and used as initial conditions for the next time step, and the model then advects a field of two,

or four, or more point masses one more time step. Again, the motion will usually not be an integral number of grid spaces, so each point source will itself give rise to several more. The result is a spreading of the initial point mass over a larger and larger area, the diameter of which increases with time; in effect, a diffusion. The effective coefficients of diffusion are proportional to the grid spacings, i.e., increasing the resolution of the grid will decrease the spurious diffusion; however, cutting the grid spacing in half will increase the core storage required for a region by four, the computing time required by about eight. (For 3-dimensional grids, these figures are, respectively, eight and sixteen.)

In contrast, the parcel-in-cell technique does not permit the spreading out of the point mass to be made permanent. Instead, with succeeding time steps, the parcel-in-cell method simply moves each point mass (or "parcel") around in the grid, spreading the mass temporarily over at most four grid locations at any one time for the purpose of computing concentrations and gradients. Each mass is returned to its true parcel position within a grid cell prior to being advected for another time step.

The model operates by interpolating wind velocities from the grid points at which they are defined to the parcel positions within the cells. Of course, if the velocity field is not uniform, interpolation to each individual parcel yields a different velocity, causing divergence or convergence of the parcels. Diffusion effects are accounted for by adding to the wind velocities at each grid point a pseudo-wind given by

$$V = - \frac{K}{C} \nabla C \qquad (3.2)$$

where K is a specified diffusion coefficient and C is concentration at the grid point. The values of concentration are obtained by temporarily spreading out the mass of each parcel

on its neighboring points of the grid, as discussed above, and then accumulating the total mass at each grid point. The concentration gradient is then obtained by any convenient finite difference scheme (in practice, centered differences). After the pseudo-wind is evaluated and combined with the given wind velocities, interpolation is used, as described above, to obtain the motion of the individual parcels.

3.3 Sample Diffusion Calculations

Since the "S^3" computer program will be used to simulate transport and diffusion of continuous plumes, a simple test case was chosen to check the operation of the program. A total of 475 lb (216 Kg) of SF_6 was assumed to be released over a 4-hr period, and transport and diffusion of the plume was calculated for a period of 20 hrs. For simplicity, a constant horizontal wind was used ($u = 7$ m/sec or 25 km/hr, $v = 0$, $w = 0$) with a constant diffusion coefficient ($K_x = K_y = 10^8 cm^2/sec$). No vertical diffusion was used ($K_z = 0$), but the effluent was assumed to be uniformly mixed in the vertical through a 2 km layer.

Figure 3.3 shows the computer print-out of concentrations at the end of the 4-hr release period. Grid points are 10 km apart, the wind is blowing from the bottom of the page toward the top, and the release point is indicated by a large dot. Concentrations are plotted in picograms of SF_6 per gram of air (pg/g). Concentration by volume (p1/1) may be obtained by dividing these values by 5. The peak concentration (56.7 pg/g averaged over a 10 x 10 x 2 km cell) occurs one cell downwind of the release point. At this time the plume is about 130 km long, and its maximum width is about 100 km at 90 km downwind.

The simulated plume at 12 hrs after the start of release is shown in figure 3.4. The peak concentration (13.5 pg/g)

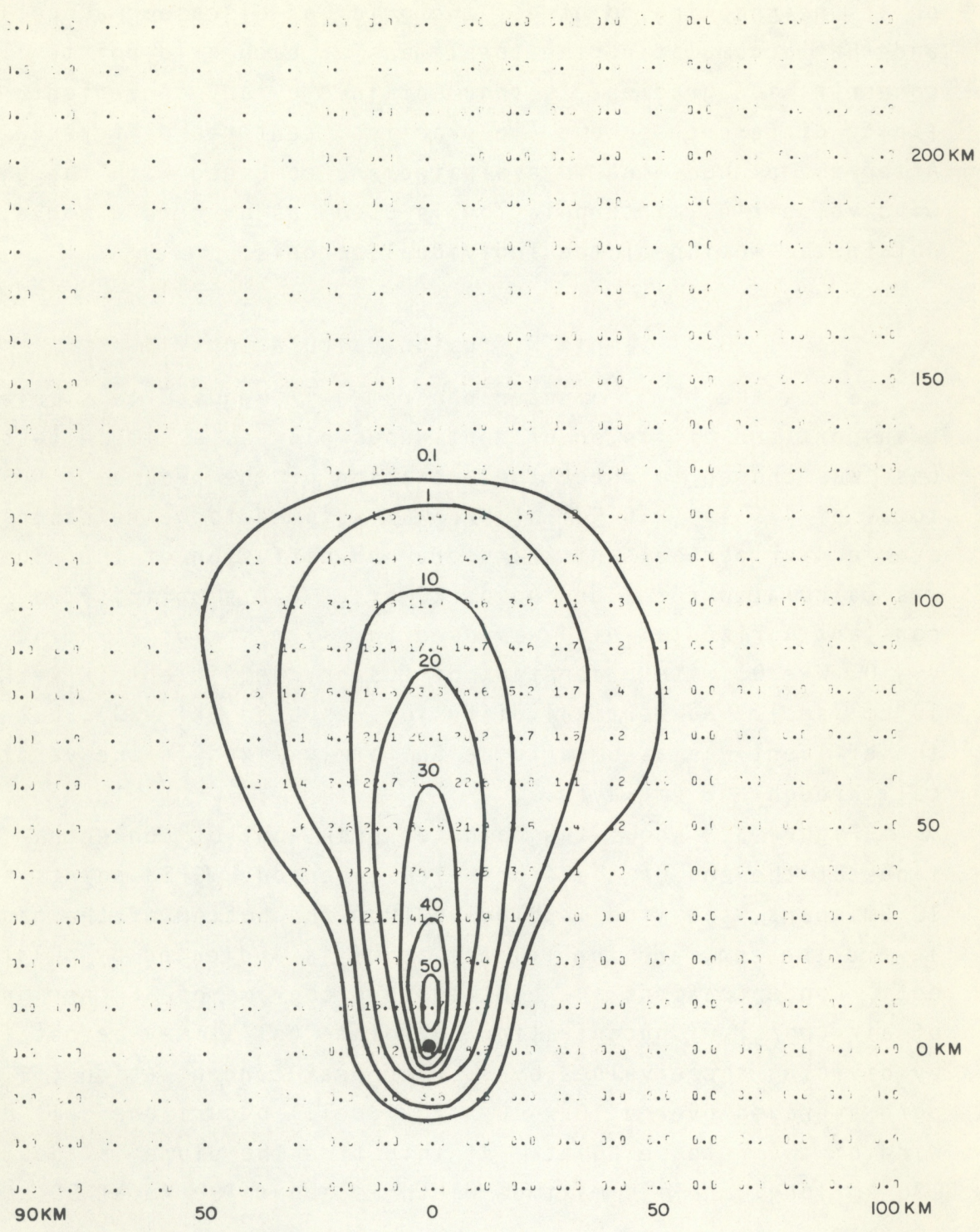

Figure 3.3. Simulated plume 4 hrs after the start of a 4-hr release.

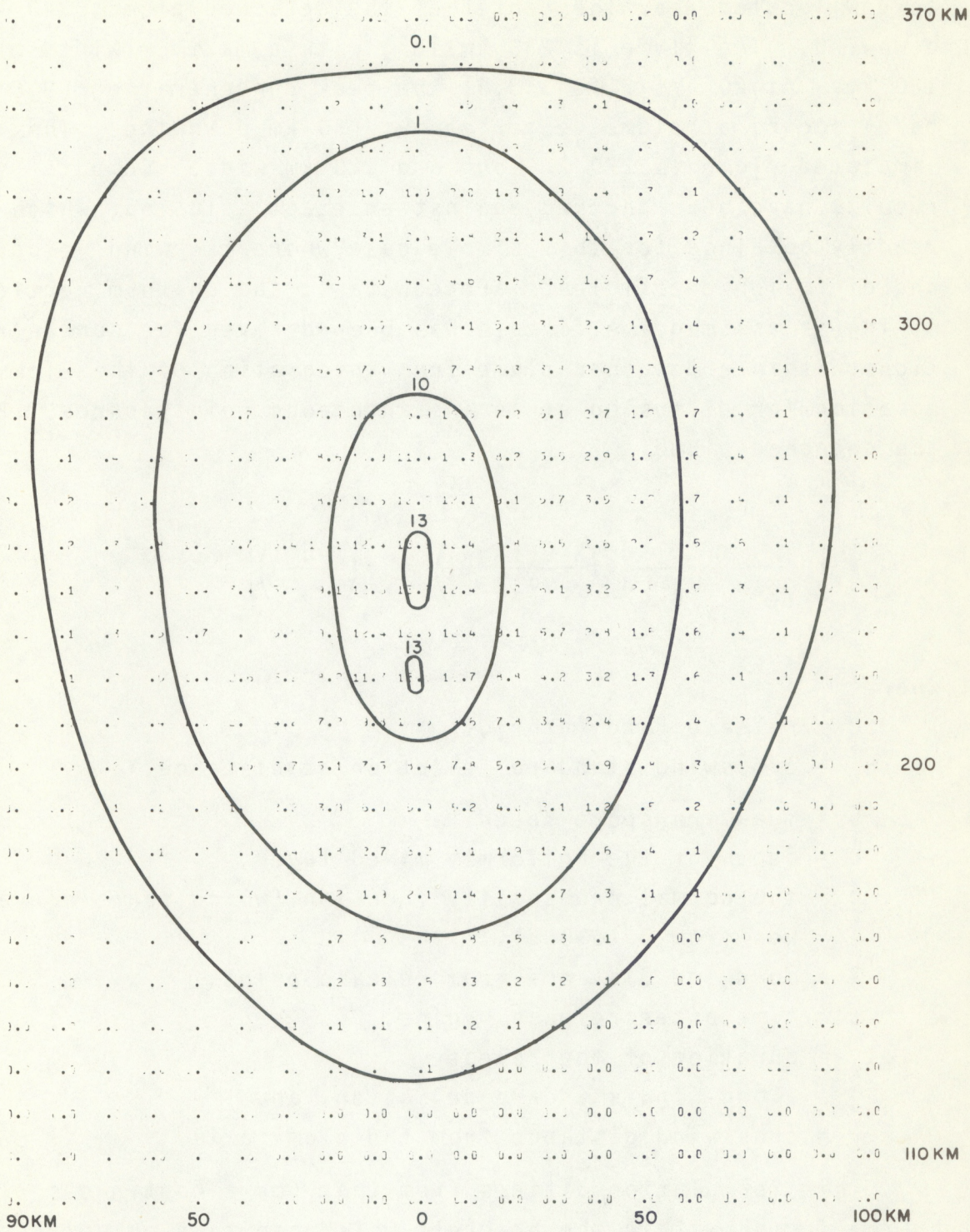

Figure 3.4. Simulated plume 12 hrs after the start of release.

is now located near the center of the detached plume, 240 km downwind. The plume is 230 km long with a maximum width of 180 km. At 20 hrs, (fig. 3.5) the peak concentration (8.6 pg/g) occurs at plume center, about 450 km downwind. The simulated plume is 270 km long and 220 km wide. Computer results have been checked against an exact solution, which is readily obtained for this simple case where the wind velocity and diffusion coefficients are constant, and uniform vertical mixing is assumed. A formula has been derived for concentrations within a detached plume from integration of the Fickian equation for diffusion of an instantaneous point source. For the detached plume,

$$\chi = \frac{Q}{\sqrt{2\pi}\,\sigma_y\,\bar{u}\,L}\left[\Phi\left(\frac{X-\bar{u}(t-t_r)}{\sigma_x}\right) - \Phi\left(\frac{X-\bar{u}\,t}{\sigma_x}\right)\right] e^{-y^2/2\sigma_y^2} \qquad (3.3)$$

where

Q = release rate (g/hr),

σ_y = crosswind standard deviation at distance X,

$\bar{u}$ = mean transport speed,

L = depth of the uniformly mixed layer,

Φ = the normal probability function (which takes on values from 0 to 0.5),

X = downwind distance from release point,

t = time after release begins,

t_r = duration of the release,

σ_x = along-wind standard deviation, and

y = crosswind distance from the plume axis.

This formulation differs from that for a continuous plume by the factor within the brackets which can take on values between zero and one.

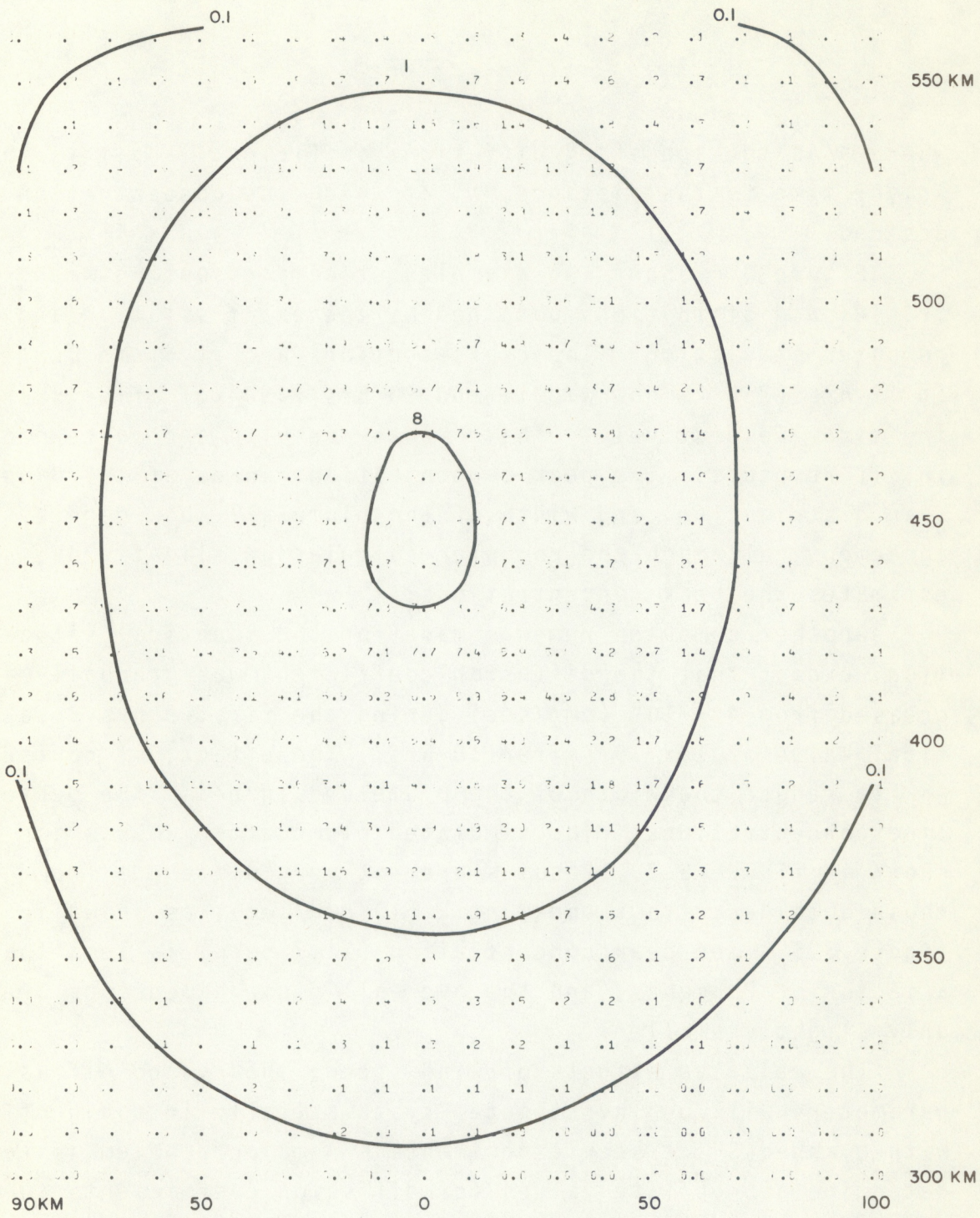

Figure 3.5. Simulated plume 20 hrs after the start of release.

Values for the standard deviation are determined from

$$\sigma = \sqrt{2\ Kt}\ , \qquad (3.4)$$

where K is the specified diffusion coefficient, and t is the travel time to the distance, X, at which the concentration is desired.

Figure 3.6 shows two examples of comparisons between crosswind distributions obtained by the exact solution and by computer simulation. The cross-sections are at plume center at 12 hrs (250 km downwind), and 20 hrs (450 km) after starting time, respectively. The computer results are quite good in all respects. The peak concentration, shape of the Gaussian distribution, and width of the plume all show good agreement, although the computer calculation slightly overestimates the peak concentrations.

Another computer run was made for the identical situation, except that the diffusion coefficient was gradually increased from 4×10^6 (cm^2/sec) during the first 3 hrs to a final value of 1×10^8 after 18 hrs. The effect, of course, was to reduce the width of the plume and increase the centerline concentrations. The simulated plume after 20 hrs is shown in figure 3.7. Results are not very different from those obtained with a constant K ($10^8 cm^2/sec$), as shown in figure 3.5. The peak concentration (14.7 pg/g) is less than a factor of 2 higher, and the over-all plume dimensions are only slightly smaller.

The relative effects of wind speed, shear, and diffusion parameters will be investigated systematically in conjunction with planned SF_6 tracer experiments. A major problem is to determine appropriate values for diffusion coefficients to be used in combination with realistic space-and-time variant wind fields.

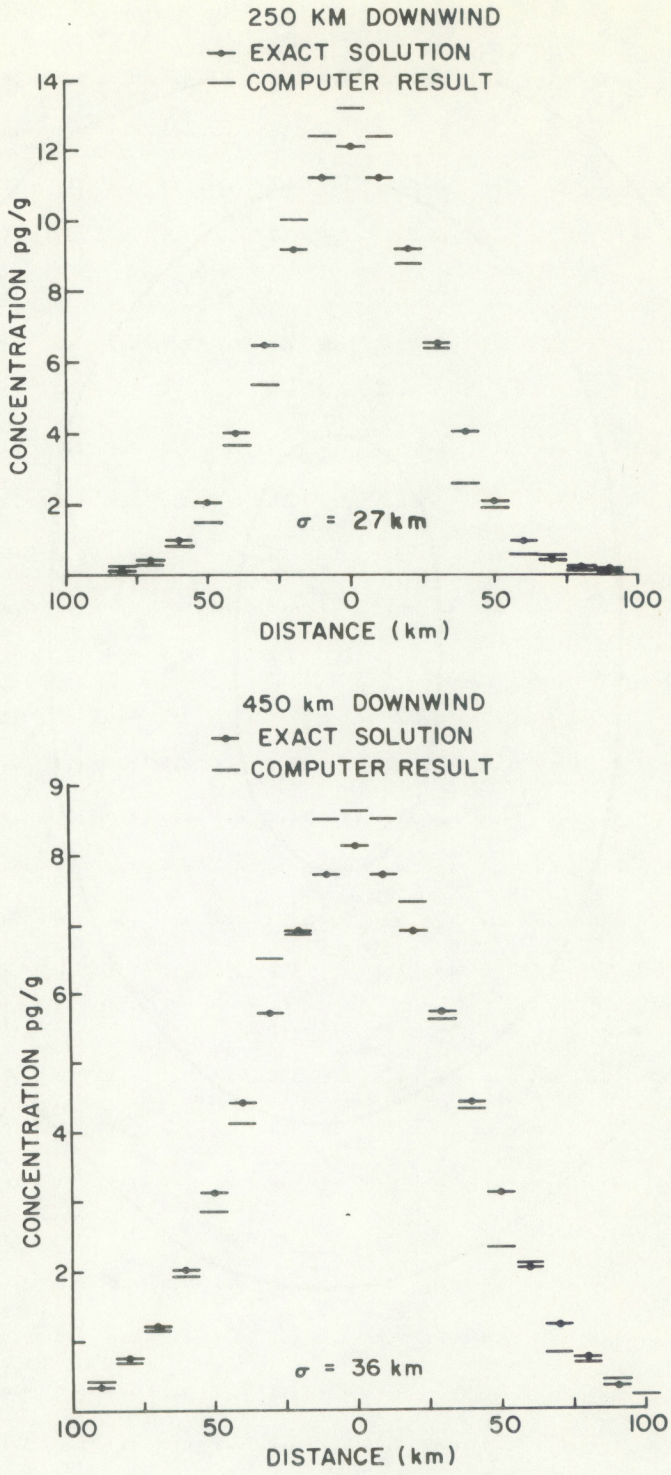

Figure 3.6. Verifications of computer-calculated cross-wind distributions.

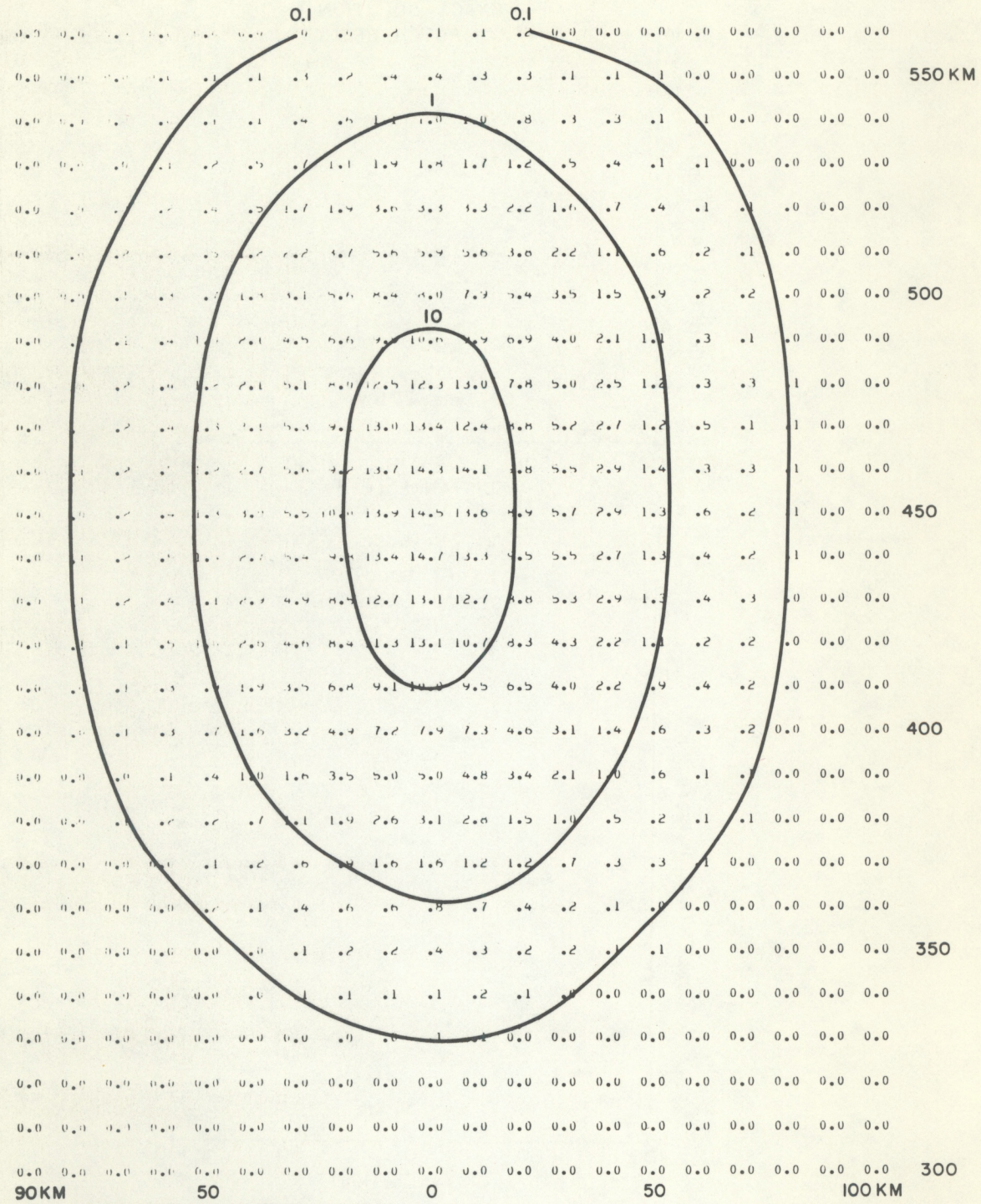

Figure 3.7. Simulated plume 20 hrs after start of release (diffusion coefficient increasing with time).

3.4 References

Clemons, C. A., A. I. Coleman, and B. E. Saltzman (1968), Concentration and ultrasensitive chromatographic determination of SF_6 for application to meteorological tracing, Environmental Science and Technology, *2*, No. 7, July 1968, pp. 551-556.

Gatz, Donald F., and J. E. Carson (1970), Sulfur hexafluoride: atmospheric background concentrations, Argonne Nat'l Lab., Radiological Physics Division Annual Report (July 1969 - Dec. 1970) ANL-7760 Part III.

Lovelock, J. E. (1971), Atmospheric fluorine compounds as indicators of air movement, Nature, *20*, April 9, 1971, p. 379.

Sklarew, Ralph C. (1970), A new approach: the grid model of urban air pollution, Systems, Science and Software, La Jolla, California, 42 pp.

Turk, A., S. M. Edwards, H. L. Mark and G. F. Collins (1968), Sulfur hexafluoride as a gas-air tracer, Environmental Science and Technology, *2*, No. 1, Jan. 1968, pp. 44-48.

4. TRAJECTORY FORECAST VERIFICATION
(J. L. Heffter)

The Air Resources Laboratory-Las Vegas is required to make trajectory forecasts in support of various programs conducted at the Nevada Test Site. As an aid, constant-pressure trajectory forecasts starting at selected locations in the western U.S. are computed twice daily at the NOAA National Meteorological Center, Suitland, Maryland, (using forecast winds obtained from the primitive equation forecast model) and transmitted to Las Vegas.

The question arises as to the confidence that can be placed in these trajectory forecasts. Emphasis, up to now, has been on verification of forecast parameters in the Eulerian system (i.e., winds at a specific location) rather than those in the Lagrangian system (i.e., trajectories). A procedure for comparing forecast trajectory endpoints to those derived from observed winds and, for placing objective confidence limits on the forecast, is being developed. Trajectory endpoint comparisons for the winter of 1970-71 (Dec., Jan., and Feb.) are reported here; comparisons for subsequent seasons will be made on a continuing basis.

4.1 Forecast Trajectories

The forecast (F) trajectory positions are given by latitude and longitude at successive 6-hr time intervals. Trajectories of interest that have been considered here are 18-hr 700-mb trajectories starting from Yucca, Nevada (UCC), based on computations using 1200Z data for a given day (1200Z on D+0). One trajectory begins at 1800Z (6 hrs after the 1200Z observation time) and ends at 1200Z on D+1 (+24 hrs) and is designated F (6, 24), as shown in figure 4.1. The other begins at 1800Z on D+1 (+30 hrs) and ends at 1200Z on D+2 (+48 hrs) and is designated F (30, 48).

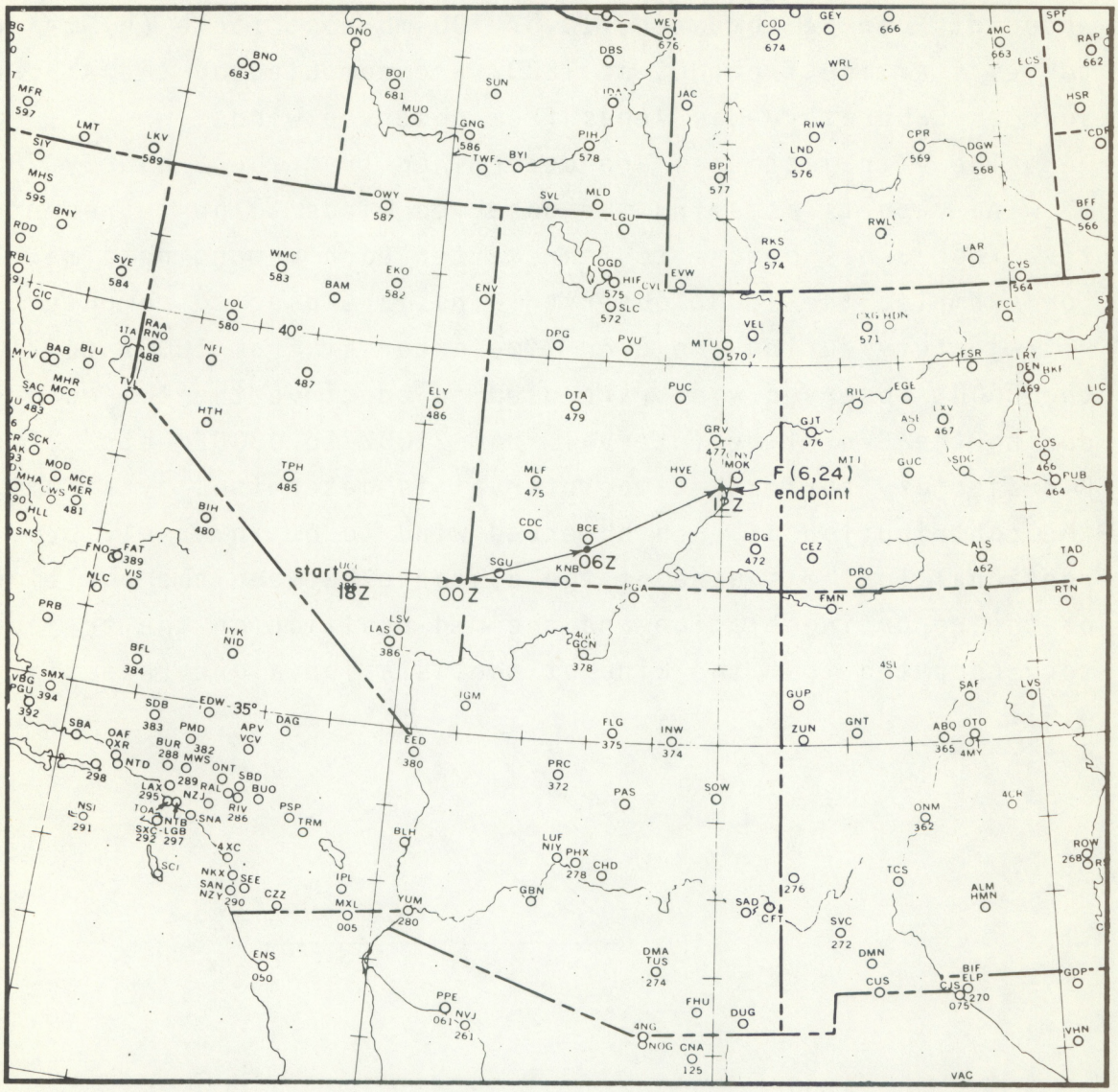

Figure 4.1. An F(6, 24) trajectory beginning 1800Z (6 hrs after the 1200Z observation time) and ending 1200Z on D+1 (+24 hrs). All trajectories considered here will be 18-hr 700-mb trajectories starting from UCC.

4.2 Post Facto Trajectories

To have some standard with which the forecast trajectory endpoints can be compared, 18-hr 700-mb post facto (P) trajectories starting from UCC at 1800Z are computed by the Air Resources Laboratory-Las Vegas from observed winds.

The P trajectories are determined from the 6-hourly 700-mb wind reports assuming the observed winds to be representative from 3 hrs before to 3 hrs after each reporting time. For example, the 1800Z observed winds are used to compute the P trajectory during the 3-hr time interval from 1800Z to 2100Z; the 0000Z observed winds are used to continue the trajectory during the 6-hr time interval from 2100Z to 0300Z; etc. The P trajectory for each time interval is determined by assuming the contribution of each observed wind to be inversely proportional to the square of the distance between the position of the reporting station and the mid-position on the trajectory computed from the wind at that station alone (see fig. 4.2).

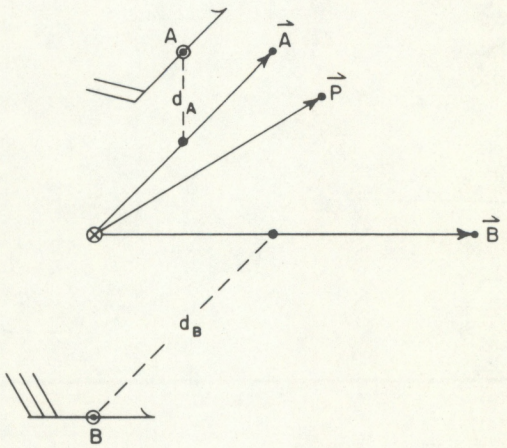

$$\vec{P} = \frac{\frac{\vec{A}}{d_A^2} + \frac{\vec{B}}{d_B^2}}{\frac{1}{d_A^2} + \frac{1}{d_B^2}}$$

Figure 4.2. The determination of a P trajectory (P) with observed winds at positions A and B. Trajectory A is computed for a given time interval from the wind at position A. d_A is the distance from position A to the mid-position on A. Similar notation applies to B.

4.3 Trajectory Comparisons

4.3.1 Procedure

The procedure for comparing endpoints of the F and P trajectories is shown in figure 4.3. The distance between F and P endpoints is expressed in component form; *along* (d_a) and *normal* to (d_n) a line of length d_F from the start to the F endpoint. (Note the conventions adopted for the signs of d_a and d_n).

The paired values d_a, d_F and d_n, d_F are determined for each trajectory comparison. A linear regression analysis is then made on each group of paired values. The plotted points and linear regression lines are shown in figures 4.4a and 4.4b for the F (6, 24) comparisons and in figures 4.5a and 4.5b for the F (30, 48) comparisons. For any F trajectory, an expected

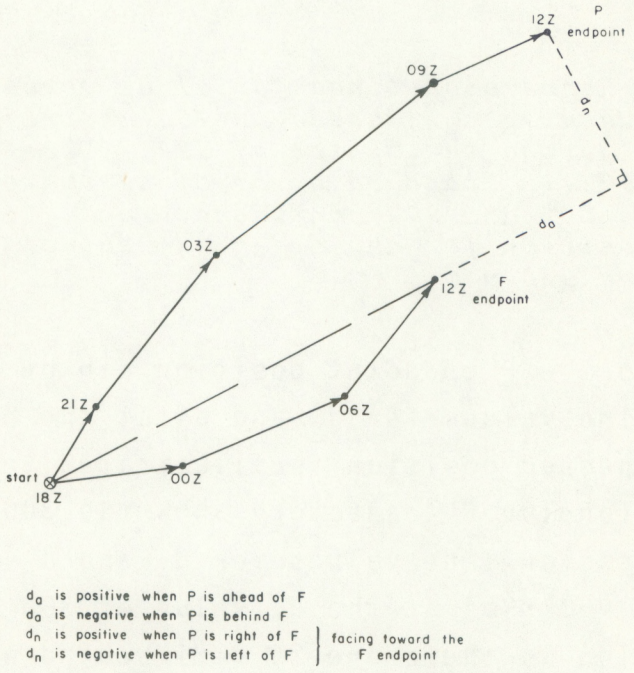

Figure 4.3. The distance between the F and P endpoints expressed in component form; along (d_a) and normal (d_n) to a line of length d_F from the start to the F endpoint. The conventions adopted for the signs of d_a and d_n are shown above.

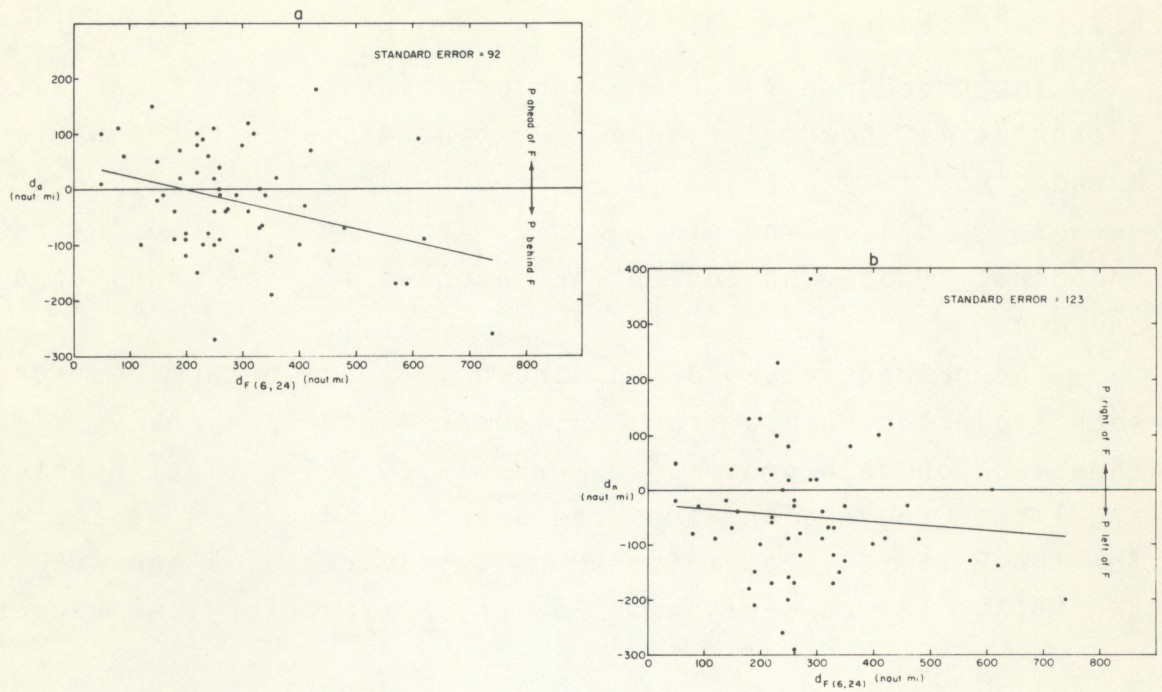

Figure 4.4. Regression lines for a) d_a versus $d_{F(6, 24)}$ and b) dn versus $d_{F(6, 24)}$ based on 700-mb trajectories starting at UCC during the winter of 1971 (Dec. 1970, Jan. 1971, and Feb. 1971). Standard error of estimate values are also given. The 50% and 90% confidence radii (applicable to the expected position for any $d_{F(6, 24)}$ value) are, respectively, 130 n mi and 230 n mi.

correction to the F endpoint position can be made using the regression line values for d_a and d_n at the proper value of d_F. This expected position is illustrated in figure 4.6. The value of d_F for the F trajectory shown is 300 n mi. From figure 4.4 regression line values for d_a and d_n are, respectively, -25 n mi and -50 n mi at the d_f value of 300 n mi. The expected position is therefore 25 n mi behind and 50 n mi left of the F endpoint position.

A homoscedastic (same scatter) normal distribution about each regression line is assumed (see discussion below) and confidence radii for an expected position are determined.

The 50 percent and 90 percent confidence radii lengths are computed from the standard error of estimate values given in figure 4.4 (Groenewoud et al., 1967). The radii (applicable to the expected position for any $d_{F(6, 24)}$ value) are, respectively, 130 n mi and 230 n mi and are illustrated in figure 4.6. Figure 4.7 shows the same technique applied to an F (30, 48) trajectory using information from figure 4.5.

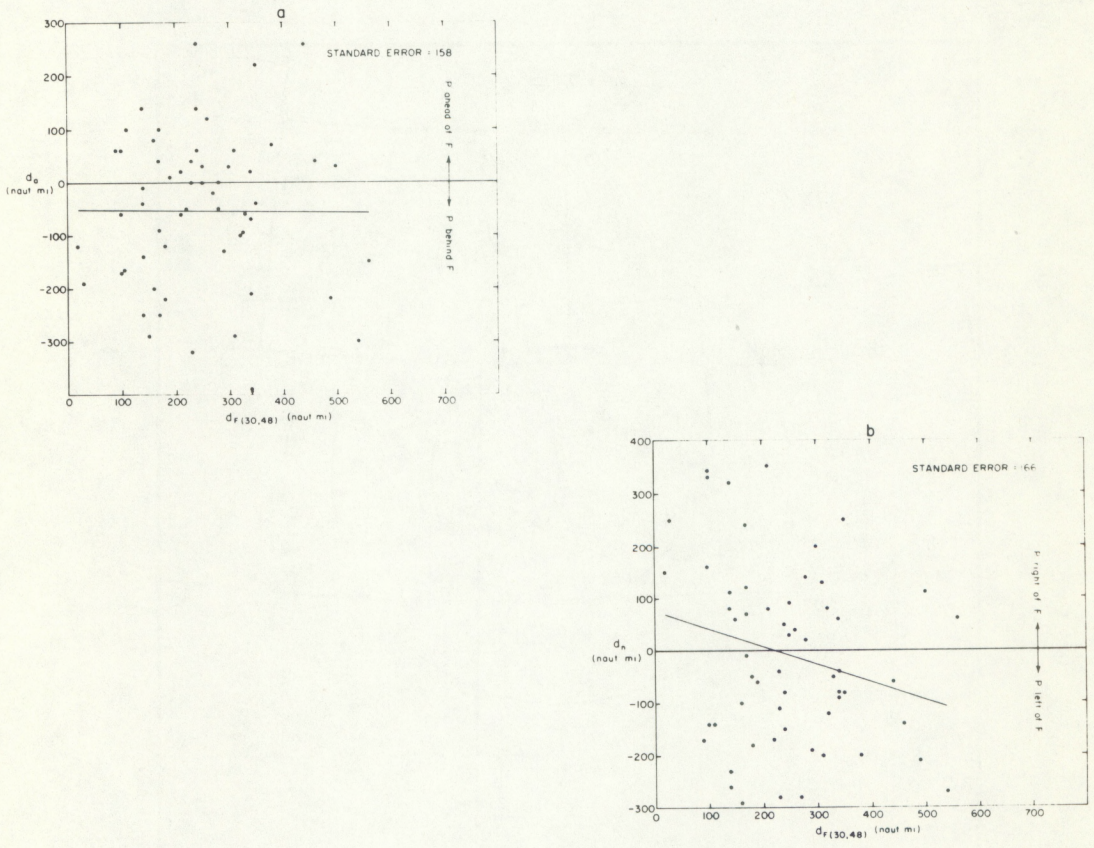

Figure 4.5. Regression lines for a) d_a versus $d_{F(30, 48)}$ and b) d_n versus $d_{F(30,48)}$ based on 700-mb trajectories starting at UCC during the winter of 1971 (Dec. 1970, Jan. 1971, and Feb. 1971). Standard error of estimate values are also given. The 50% and 90% confidence radii (applicable to the expected position for any $d_{F(30,48)}$ value) are, respectively, 190 n mi and 340 n mi.

It might also be interesting to compute the probability that a trajectory endpoint would fall within a circular area other than around the expected position. This type of computation can be made using the information given in figures 4.4 or 4.5 as input to the tables in Groenewoud et al. (1967). As an example, given the F (6, 24) trajectory in figure 4.6, the probability that a trajectory endpoint would fall within a 30-n mi radius of Lander, Wyoming, (LND) is found to be 0.003.

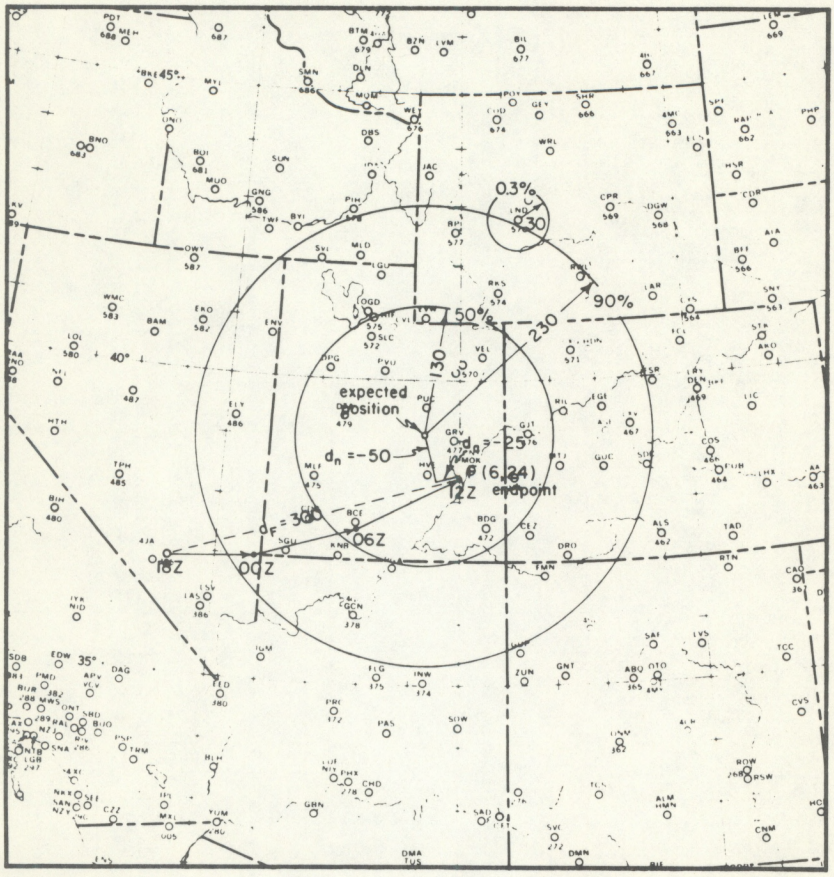

Figure 4.6. An example of the expected position and confidence radii (determined from fig. 4.4) for the F(6, 24) trajectory shown above with a d_F value of 300 n mi. Included is the computed probability of a trajectory endpoint within a 30 n mi radius of Lander, Wyoming.

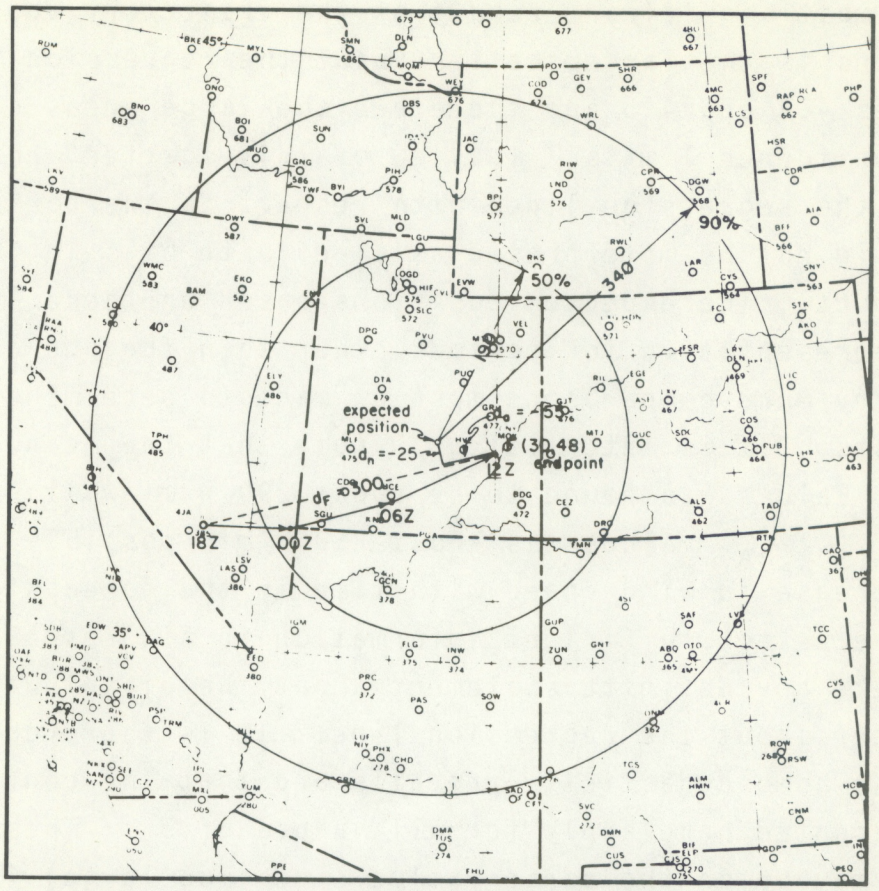

Figure 4.7. An example of the expected position and confidence radii (determined from fig. 4.5) for the F (30, 48) trajectory shown above with a d_F value of 300 n mi.

4.3.2 Discussion

The comparison between F and P endpoints has certain limitations. The P trajectories computed here are subject to errors because of the dependence on the distribution and number of wind reports available, and the time intervals and weighting technique used. They can, therefore, only be considered as approximations of actual constant level trajectories.

The most significant result of the trajectory endpoint comparisons is the large scatter about the regression lines in figures 4.4 and 4.5 and therefore the large areas covered by the confidence limits. In view of this scatter, the positions of the regression lines with respect to the horizontal axes should not be interpreted as a definite bias in the forecast product. The expected positions based on these lines may not be representative for periods other than the one considered. Many more comparisons must be made to determine if a bias exists. It is interesting to note that the mean of the $d_{F(6, 24)}$ values was found to be about 290 n mi while the mean of the $d_{F(30, 48)}$ values was about 250 n mi, possibly indicating a decrease in wind speed with time in the forecast product.

There is not sufficient information in figures 4.4 and 4.5 to make any definite statement about the distribution of the scatter about the regression line. It is therefore assumed that homoscedasticity prevails and that the confidence radii presented here apply for all values of d_F. These radii, however, may be on the conservative side (too large) for small d_F (less than about 100 n mi).

It should finally be emphasized that the large areas covered by the confidence limits, as illustrated in figures 4.6 and 4.7 leave little doubt that a forecast trajectory must be used with caution.

4.4 References

Groenewoud, C., D. C. Hoaglin, J. A. Vitalis (1967), Bivariate normal offset circle probability tables, Cornell Aeronautical Laboratory, Inc., Buffalo, New York.

5. ATMOSPHERIC NUCLEAR DEBRIS

(K. Telegadas, R. J. List, and J. L. Heffter)

The Limited Nuclear Test Ban Treaty (1963) has not resulted in a complete cessation of atmospheric nuclear testing. Although the scale of testing has been drastically reduced since 1962, sporadic atmospheric nuclear testing by France and China has provided unique opportunities for meteorological analysis. These tests have injected nuclear debris into different regions than did the earlier tests, the northern temperate-latitude stratosphere and the troposphere and stratosphere near the Tropic of Capricorn. This debris has been injected into an atmosphere relatively free of debris from earlier tests, and the injections have occurred as single events or over a short time span. These characteristics are particularly useful in meteorological investigations.

5.1 French and Chinese Stratospheric Debris

The two French megaton-yield tests of August 24 and September 8, 1968, (22°S), and the Chinese megaton-yield test of December 27, 1968, (40°N) provided a unique opportunity to investigate lower stratospheric motions in each hemisphere and the interaction in the lower tropical stratosphere. Isotopic ratios made it possible to identify debris from each of the source regions. The study revealed that the tropospheric Hadley cell circulation also plays an important role in the lower stratosphere. The results of the study have been published in the Journal of Geophysical Research, Vol. 76, no. 21, pp. 5018-5024, July 20, 1971, in a paper by K. Telegadas, entitled "The upper portion of the Hadley cell circulation as deduced from the 1968 French and Chinese nuclear tests." The abstract follows:

French and Chinese nuclear testing in 1968 provided an opportunity for studying stratospheric

transport processes. The French tests of August and September 1968 and the Chinese test of December 1968 provided radioactive tracers to follow air motions in the lower stratosphere of each hemisphere. The two sources are readily distinguishable by fission product ratios (e.g., Zr-95/Ce-144). Information on interhemispheric exchange in the upper troposphere and lower stratosphere has been developed by the analysis of air-filter samples obtained by aircraft and balloons. The meridional transport of radioactive debris into the lower equatorial stratosphere from two sources is qualitatively explained by a mean meridional circulation superimposed on large-scale mixing processes. It is further suggested that the mean circulation is an extension of the tropospheric Hadley Cell into the lower stratosphere.

5.2 French and Chinese Tropospheric Debris

The AEC Health and Safety Laboratory, New York, maintains an extensive ground-level air sampling network providing data on the concentration of several radionuclides in ground-level air averaged over one-month periods. These sampling stations extend from 77°N to 65°S and are principally located near the 80°W meridian, with several stations at other longitudes. Similar data from other longitudes are available from the U.K. Atomic Energy Research Establishment network. Using concentration and nuclide ratio data, it is possible to distinquish the several sources of radioactivity in surface air and to delineate the cross-equatorial flow of French debris in 1968 and of the Chinese debris in 1970.

The report on this research is in the Journal of Geophysical Research (vol. 77, no. 6, pp. 1004-9, Feb. 20, 1972) in an article by K. Telegadas, "Atmospheric radioactivity along the HASL ground-level sampling network, 1968 to mid-1970, as an indicator of tropospheric and stratospheric sources". The abstract follows:

> Radioactivity concentrations and activity ratios in air sampled at ground-level locations are useful

in correlating the latitudinal spread of nuclear debris with a tropospheric or stratospheric source. In late 1968 and again in late 1969, China detonated a high-yield nuclear device in the northern hemisphere (40°N), and France conducted a nuclear test series (22°S) in mid-1968 and in mid-1970. An examination of the Zr-95 concentrations and Zr-95 to Ce-144 activity ratios indicates several time and space regions with similar radioactivity characteristics that can be related to one of these specific sources of debris.

5.3 Debris from Nuclear Cratering Experiments

As part of the Plowshare Program, a nuclear excavation experiment was conducted at the Nevada Test Site on December 8, 1968. The 31-kiloton yield device produced a debris cloud that rose to 19,000 ft MSL. The cloud moved generally northward and eastward and was tracked and sampled by aircraft for a period of several days. A report on the characteristics of the airborne Schooner cloud at long distances is being prepared by J. L. Heffter.

5.4 Atmospheric Radioactivity and the Photographic Industry

In 1958, the AEC assigned this office the responsibility of keeping the photographic industry alerted to possible contamination from nuclear tests. The industry has been kept informed of potential contamination situations by direct contact with the National Association of Photographic Manufacturers. Estimates of debris trajectories and rainfall scavenging are provided. During FY 71, information concerning the Chinese test of October 14, 1970, and the inadvertent venting at the Nevada Test Site on December 18, 1970, was provided. A letter to the laboratory from the National Association of Photographic Manufacturers dated December 23, 1970,

reads, in part:

> Thank you for your cooperation in alerting the National Association of Photographic Manufacturers to atmospheric atomic fallout this past week.
>
> Through your efforts, NAPM was able to alert its members and thereby avoid costly production losses in photographic film and chemicals.

6. MOLECULAR SIEVE CARBON-14

(T. E. Ashenfelter and K. Telegadas)

A new sampler for collection of atmospheric CO_2 utilizing molecular sieve adsorption has been developed and flown on operational USAEC balloon flights over San Angelo, Texas, ($31^{\circ}N$) at altitudes ranging from 21 to 37 km. The total weight of this sampler and molecular sieve material is approximately 30 kg. Depending on altitude, between 1 and 5 liters of CO_2, sufficient for accurate C-14 measurements, were collected on each mission. Based on 24 measurements in 1968-1970, the upper stratosphere has small vertical gradients of excess C-14 at $31^{\circ}N$.

6.1 Introduction

Carbon-14 with a half-life of about 5700 years has always been present in the earth's atmosphere. Atmospheric nuclear detonations have brought about an increase in the atmospheric content of C-14 referred to as "excess" C-14. Since atmospheric C-14 occurs principally in the form of gaseous CO_2, it can serve as a better tracer of atmospheric motions than particulate radioactivity which may separate from its associated air mass by gravitational settling (Telegadas and List, 1969).

The use of molecular sieves for collection of stratospheric CO_2 samples by balloon-borne devices was pioneered by the General Mills Electronic Group for the Air Force in hopes of replacing their balloon-borne whole air sampler (Steinberg and Rohrbough, 1962). Two inter-comparison tests between the whole air and molecular sieve samplers were undertaken in 1964. The C-14 analysis indicated less than a 2 percent difference between the systems (Fergusson, 1966).

The new design of the C-14 sampler reduced its overall weight and size to such an extent that it could readily be flown on the AEC-sponsored balloon-borne particulate sampling missions.

6.2 Description of Sampler

The molecular sieve sampling unit was designed to collect CO_2 at altitudes ranging from 20 to 37 km using a balloon as the sampling platform. Important features of this sampler are shown in figure 6.1. The complete system, containing the molecular sieve adsorbent, helium primary gas supply, and necessary containers and hardware, weighs about 30 kg. It is lifted to a predetermined float altitude with the sampling unit sealed. At altitude, the inlet and outlet doors are opened and air is pumped through two beds containing Linde Type 4A Molecular Sieve 1/8 in diameter pellets

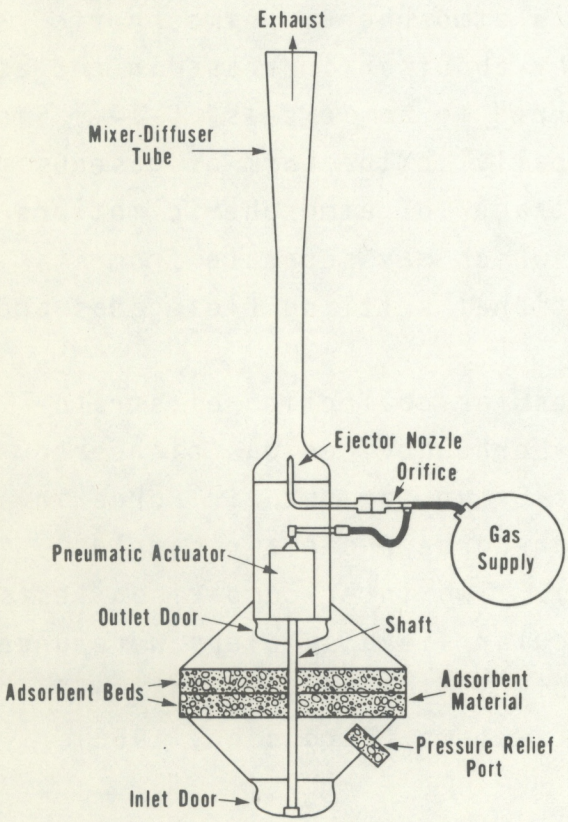

Figure 6.1. Schematic diagram of the molecular sieve sampler.

(Sinclair, 1968) for a predetermined time. An air ejector pump is used in which a jet of high velocity primary gas is ejected into a mixing tube which then expands and by turbulent exchange of momentum creates a partial vacuum causing ambient air to be drawn through the molecular sieve media. When the primary gas is expended, the doors automatically close and the system descends by parachute to the surface. This system has proven much simpler, lighter and more reliable than use of electrically powered fans, and it eliminates contamination from motors with a potential carbon source. The molecular sieve pellets are returned to Argonne National Laboratory for quantitative determination of adsorbed CO_2, C-14 analysis and regeneration (Ashenfelter et al., 1972).

The first 12 test flights of the C-14 sampler at varying altitudes had a PR-3 flowmeter (Wood et al., 1965) mounted on the air inlet. Volumes computed from flowmeter data were within 2 percent of the CO_2 analysis, based upon a 315 ppm concentration. The expected volume based on the chamber test data and these experimental flights for a two-layer adsorbent bed of 40.6 cm diameter and 3.8 cm thickness for each bed filled with 2.27 kg of Linde Type 4A Molecular Sieve pellets is given in table 6.1.

Table 6.1. Simulated Flight Conditions for Operational C-14 Sampler

Sampling altitude (km)	21	24	27	32	37
Sampling interval (min)	75	105	175	135	180
Standard cubic meters of propellant gas required[1]	1.7	2.4	4.0	3.1	4.1
Expected Bed Temp (°C)	-45	-42	-40	-35	-20
Anticipated Volume[2] (liters of CO_2 at STP)	5.3	5.2	5.6	2.2	1.3

[1]At 50 psig dynamic.

[2]Volume dependent on bed temperature.

6.3 Results and Discussion

Excess C-14 obtained from 21 to 37 km altitude at San Angelo, Texas, (31°N) is given in table 6.2. These results are also shown in figures 6.2 and 6.3 for comparison with tropospheric and stratospheric aircraft samples (NOAA, 1971).

The tropospheric aircraft data for February 1969, figure 6.2, indicate virtually no concentration gradients in the tropospheric reservoir. In the lower stratosphere, the gradients are downward and equatorward. The March 1969 balloon and February 1969 aircraft values seem to be compatible near 21 km and 31°N, the only place at which a comparison can be made.

Table 6.2. Excess C-14 Collected over San Angelo, Texas, 31°N

Date	Altitude (km)	CO_2 Volume (liters STP)	Excess C-14	
			dpm/gC	10^5 atoms/g air
3/13/69	20.7	4.8	28.0	158
7/10/69	20.9	6.1	26.5	149
9/04/69	21.3	6.8	24.5	138
1/07/70	21.4	2.9	22.7	128
3/12/70	21.3	3.9	24.4	138
7/01/69	24.3	5.9	24.8	140
9/06/69	24.3	5.9	27.0	152
1/08/70	24.6	4.4	25.8	146
3/13/70	24.2	4.1	25.7	145
7/08/69	27.3	5.4	28.0	158
9/15/69	28.1	4.1	25.2	142
1/16/70	27.1	3.2	28.4	160
3/17/70	27.2	3.8	26.9	152
1/21/69	29.3	3.3	27.4	155
2/11/69	29.9	1.1	24.9	140
3/21/69	29.6	2.9	27.8	157
5/18/69	32.0	1.6	27.0	152
7/09/69	32.1	0.8	26.7	151
9/14/69	32.8	0.9	27.3	154
1/12/70	32.6	0.9	23.4	132
3/23/70	33.0	1.1	23.9	135
5/24/68	36.6	0.8	27.7	156
11/05/68	36.3	0.7	26.3	148
9/16/69	36.5	0.8	25.7	145

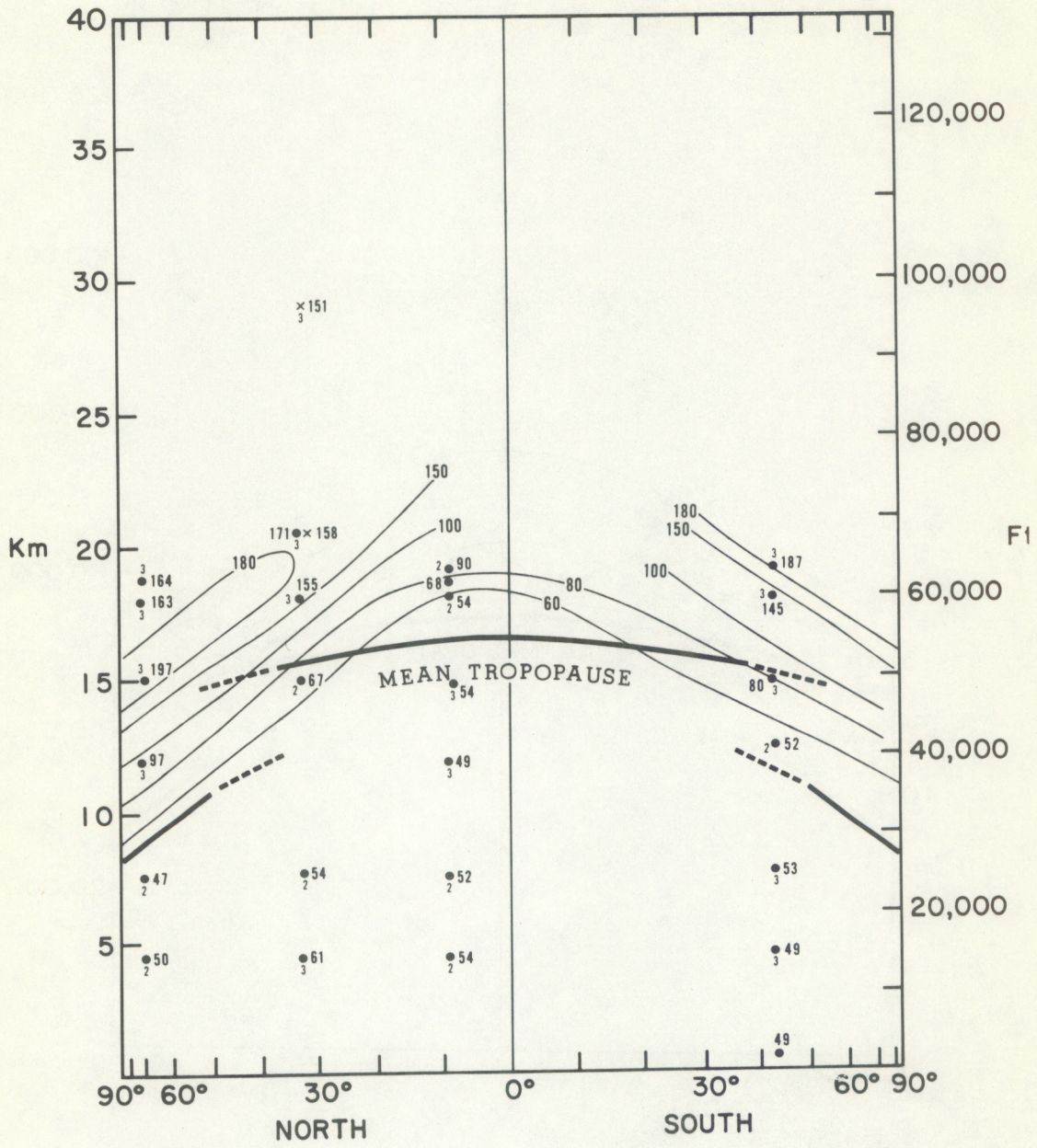

Figure 6.2. Mean excess C-14 distribution for January - March 1969. Isolines show average concentration in units of 10^5 atoms per gram of air. Dots represent location of aircraft samples collected in February 1969 while crosses denote balloon samples collected between January and March 1969. Subscript numbers are the number of samples from which the mean concentration was computed.

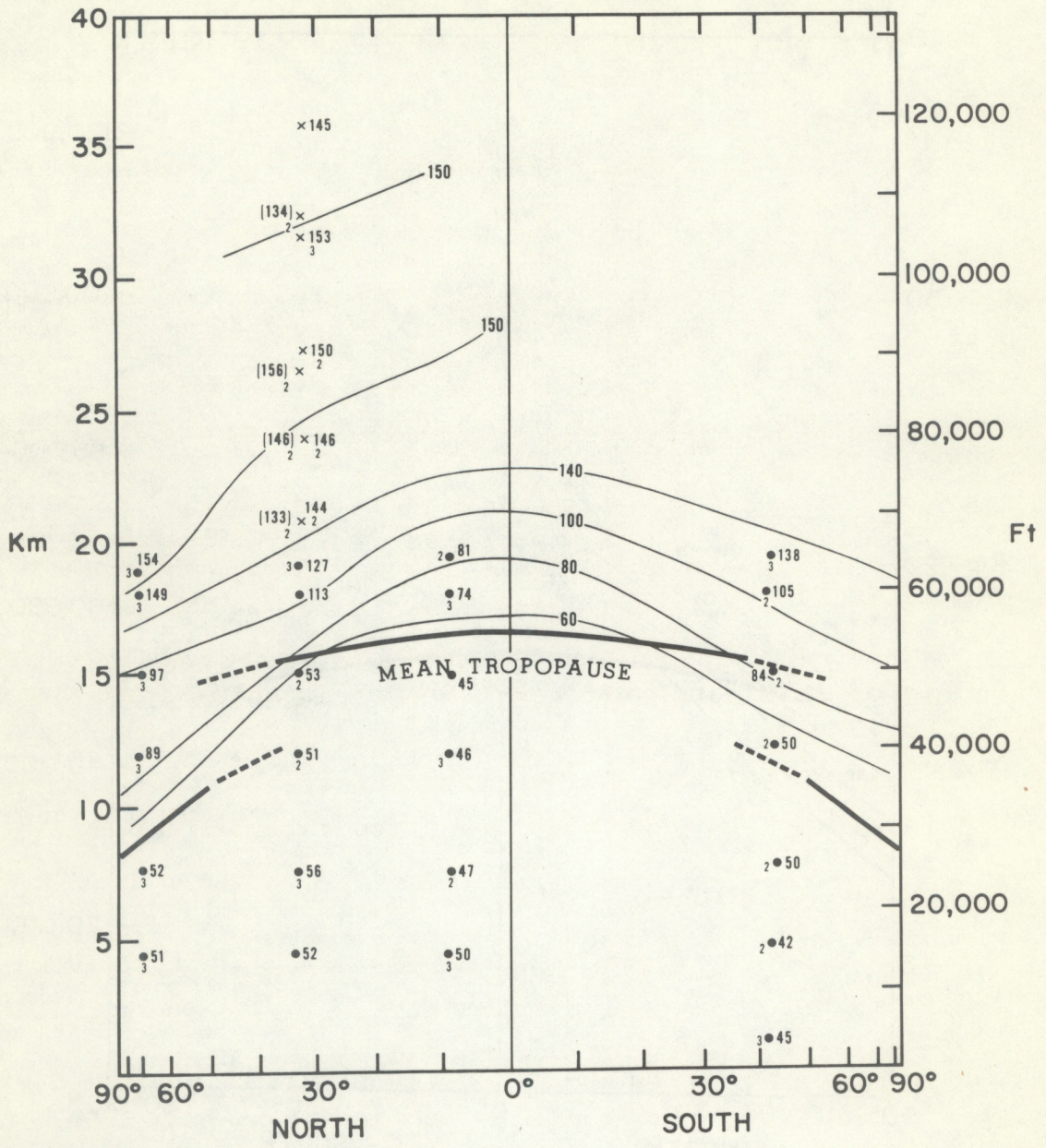

Figure 6.3. Mean excess C-14 distribution for May - September 1969. Isolines show average concentration in units of 10^5 atoms per gram of air. Dots represent location of aircraft samples collected in July 1969 while the crosses denote balloon samples collected between May and September 1969. Numbers in brackets represent balloon samples collected between January and March 1970. Subscript numbers are the number of samples from which the mean concentration was computed.

Aircraft data for July 1969, shown in figure 6.3, again indicate a well-mixed tropospheric reservoir and a fairly well-mixed lower stratospheric reservoir. The balloon data at 31°N indicate virtually no C-14 gradient between 21 and 36 km.

Since July 1970, the C-14 sampler has been successfully flown operationally on the USAEC-sponsored particle-collection missions between 21 and 37 km at Eielson AFB, Alaska (65°N), Sioux City, Iowa (42°N), San Angelo, Texas (31°N), Albrook, Canal Zone (9°N), Longreach (23°S) and Mildura (34°S) Australia. A large body of data will be reported in the Health and Safety Laboratory *Quarterly Summary Reports* as have previous data from the whole-air balloon samples (U.S. Government, 1967).

It is very likely that this light weight sampler may be used for other atmospheric gases such as SO_2, NO_x, water vapor, and hydrocarbons. Laboratory studies of the adsorption characteristics of the currently used molecular sieve and other types of adsorption media will be necessary to determine its full potential. This sampler can accommodate varying thicknesses of adsorbent beds with minor modification of the sampling unit.

6.4 References

Ashenfelter, T. E., J. Gray, Jr., R. E. Sowl, M. Svendson, and K. Telegadas (1972), A light weight molecular sieve sampler for measuring stratospheric carbon-14, J. Geophys. Res., *77*, No. 3, pp. 412-419.

Fergusson, G. J. (1966), private communication.

National Oceanic and Atmospheric Administration (1971), Carbon-14 measurements in the atmosphere, Health Safety Lab., U.S. AEC Publ. HASL-242, April 1971.

Sinclair, P. M. (1968), Molecular sieves, zealous zeolites, Industrial Research 10, No. 8, pp. 60-64.

Steinberg, S., and S. F. Rohrbough (1962), The collection and measurement of carbon dioxide and water vapor in the upper atmosphere, J. Appl. Meteor., *1*, No. 13, pp. 418-421.

Telegadas, K., and R. J. List (1969), Are particulate radioactive tracers indicative of stratospheric motions? J. Geophys. Res., *74*, No. 6, pp. 1339-1350.

U.S. Government (1967), Carbon-14 measurements in the atmosphere, Health Safety Lab., U.S. AEC Publ. HASL-174, III-42-III-70, Jan. 1967.

Wood, R. W., L. R. Graf and L. V. Nelson (1965), Development and calibration of the PR-3 flowmeter, COO-401-118, Applied Science Division, Litton Industries, Minneapolis, Minn.

7. SEASONAL INVENTORIES OF EXCESS CARBON-14
(Kosta Telegadas)

Extensive measurements of excess carbon-14 (C-14 due to nuclear weapons testing) in the form of CO_2 are available. The distribution of this isotope as a function of time and space can be used as a tracer for atmospheric motions and for estimating the exchange rate of CO_2 between the atmosphere and the oceans and biosphere.

The data from samples collected aboard U.S. aircraft and balloons in both the stratosphere and troposphere using whole air samplers (Hagemann et al., 1965; ESSA, 1966, 1968, 1969; NOAA, 1971) were presented in the form of seasonal latitudinal cross-sections and tables of the burden for various atmospheric compartments for the period March 1955 to July 1969 (Telegadas, 1971). In this chapter only certain general observations will be made from these data.

7.1 Stratospheric Inventories

The seasonal stratospheric burdens of excess C-14 from March 1955 to July 1969 have been calculated from the distributions presented by Telegadas (1971). In this study the stratosphere has been divided into 8 compartments (4 in each hemisphere), as shown schematically in figure 7.1. This partitioning and the latitudinal cross-sections can be used to ascertain where the largest uncertainties exist in the stratospheric inventories due to lack of data. The seasonal burden calculations for each compartment are summarized in table 7.1. Parentheses signify compartments with particularly large uncertainty in the calculated burden.

The world stratospheric burden to 100,000 ft is shown graphically in figure 7.2. The hatched boxes at the top of this figure indicate the periods of high yield atmospheric

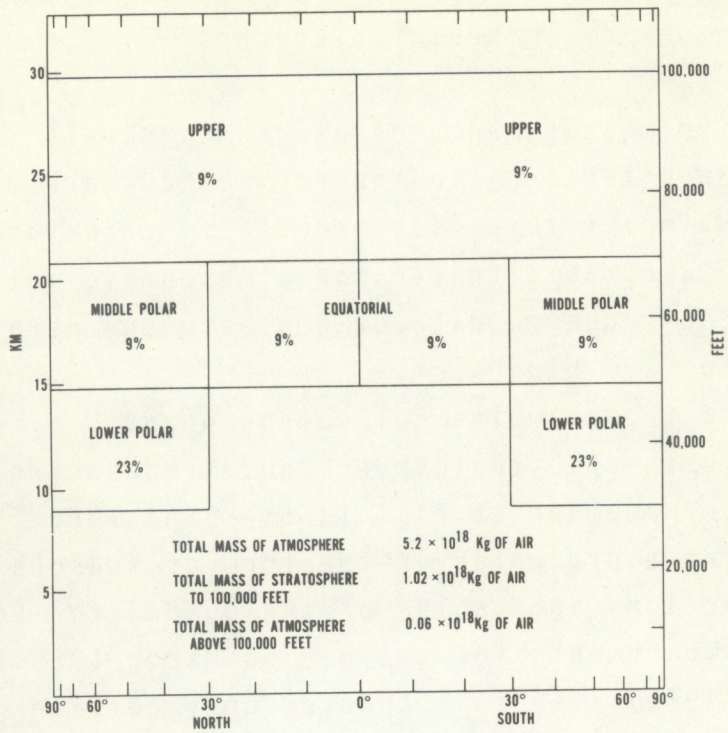

Figure 7.1. Schematic stratospheric compartments (numbers represent percent of total stratospheric mass to 100,000 ft).

nuclear testing. The numbers below the hatched areas indicate the total megatonnage *equivalent* of C-14 atoms released to the atmosphere. Machta et al. (1963) assumed that a one-megaton total yield air burst introduces 2×10^{26} C-14 atoms into the atmosphere, while similar yield surface burst introduces one-half this amount. The total yield of air and surface bursts for various test series (U.S. Weather Bureau, 1964; U.S.A.E.C., 1968; Krey et al., 1969) with Machta's assumptions indicate, for example, that for the period 1955-1956, 19 megatons equivalent were released to the atmosphere; this converts to 38×10^{26} C-14 atoms.

The high altitude whole-air C-14 balloon program terminated in July 1966; therefore, the total stratospheric burden to 100,000 ft could not be computed beyond this period. Enough

Table 7.1. Excess C-14 Inventory (atoms × 10^{26})

Quarter	Stratosphere									
	Northern Hemisphere					Southern Hemisphere				
Latitude Alt (k ft)	0-90 70-100	30-90 50-70	0-30 50-70	30-90 30-50	Total	0-90 70-100	30-90 50-70	0-30 50-70	30-90 30-50	Total
3/55- 5/55	17	11	3	5	36	8	(3)	1	(2)	(14)
6/55- 8/55	16	10	3	4	33	9	(2)	1	(1)	(13)
9/55-11/55	19	9	2	5	35	22	(3)	1	(2)	(28)
12/55- 2/56	17	11	3	6	37	10	(2)	2	(1)	(15)
3/56- 5/56	15	11	3	5	34	6	(2)	1	1	(10)
6/56- 8/56	15	8	3	4	30	10	(6)	3	2	(21)
9/56-11/56	18	10	6	4	38	12	(7)	5	2	(26)
12/57- 5-57	20	16	5	7	48	11	(6)	3	2	(22)
3/57- 5/57	20	16	4	8	48	10	(3)	1	2	(16)
6/57- 8/57	18	13	4	6	41	13	(5)	2	3	(23)
9/57-11/57	16	15	4	6	41	11	(8)	3	2	(24)
12/57- 2/58	15	13	5	7	40	11	(5)	3	3	(22)
3/58- 5/58	15	12	4	10	41	12	(6)	3	5	(26)
6/58- 8/58	16	14	8	9	47	12	(9)	6	5	(32)
9/58-11/58	17	13	13	8	51	14	10	7	8	39
12/58- 2/59	23	20	13	17	73	16	(8)	9	8	(41)
3/59- 5/59	24	19	(9)	23	(75)	(15)	9	(7)	9	(40)
6/59- 8/59	22	16	(7)	11	(56)	(13)	9	(7)	10	(39)
9/59-11/59	21	15	(6)	9	(51)	--	-	-	--	--
12/59- 2/60	23	16	(6)	(14)	(59)	--	-	-	--	--
3/60- 5/60	20	13	6	12	51	(11)	7	(5)	7	(30)
6/60- 8/60	21	13	(7)	(13)	(54)	(11)	8	(6)	8	(33)
9/60-11/60	17	11	4	8	40	(10)	8	(4)	7	(29)
12/60- 2/61	--	--	-	--	--	--	-	-	--	--
3/61- 5/61	16	11	(6)	13	(46)	(11)	8	(6)	8	(33)
6/61- 8/61	15	(12)	6	(10)	(43)	--	-	-	--	--
9/61/11-61	13	(18)	(11)	(16)	(58)	(10)	6	(6)	7	(29)
12/61- 2/62	--	--	-	--	--	--	-	-	--	--
3/62- 5/62	20	75	11	44	150	(10)	8	7	9	(34)
6/62- 8/62	42	70	34	25	171	--	-	-	--	--
9/62-11/62	42	(106)	57	(40)	(245)	(16)	12	(23)	15	(66)
12/62- 2/63	60	144	39	67	310	(15)	10	(9)	12	(46)
3/63- 5/63	64	113	29	94	300	(18)	9	(10)	12	(49)
6/63- 8/63	66	86	39	52	243	(20)	10	(13)	15	(58)
9/63-11/63	66	78	29	42	215	(18)	11	(13)	15	(57)
12/63- 2/64	52	71	25	55	203	(15)	11	(11)	15	(52)
3/64- 5/64	39	55	20	62	176	(15)	9	(10)	15	(49)
6/64- 8/64	41	38	19	30	128	(15)	11	(12)	17	(55)
9/64-11/64	39	37	16	27	119	(14)	11	(11)	15	(51)
12/64- 2/65	38	35	14	26	113	(19)	11	(11)	16	(57)
3/65- 5/65	33	29	13	26	101	(15)	11	(11)	18	(55)
6/65- 8/65	33	24	13	22	92	(15)	13	(12)	19	(59)
9/65-11/65	31	24	11	22	88	(15)	12	(10)	19	(56)
12/65- 2/66	26	25	12	25	88	(18)	14	(9)	17	(58)
3/66- 5/66	22	21	11	25	79	(14)	12	(9)	17	(52)
6/66- 8/66	23	19	10	21	73	(17)	12	(9)	17	(55)
9/66-11/66	--	17	10	19	--	--	-	-	--	--
1/67	--	19	8	21	--	--	11	(9)	16	--
7/67	--	15	10	20	--	--	12	(10)	16	--
1/68	--	17	10	19	--	--	11	(9)	15	--
6/68	--	14	8	17	--	--	11	(8)	15	--
2/69	--	14	7	17	--	--	13	(7)	15	--
7/69	(12)	11	7	15	45	(11)	10	(7)	13	(41)

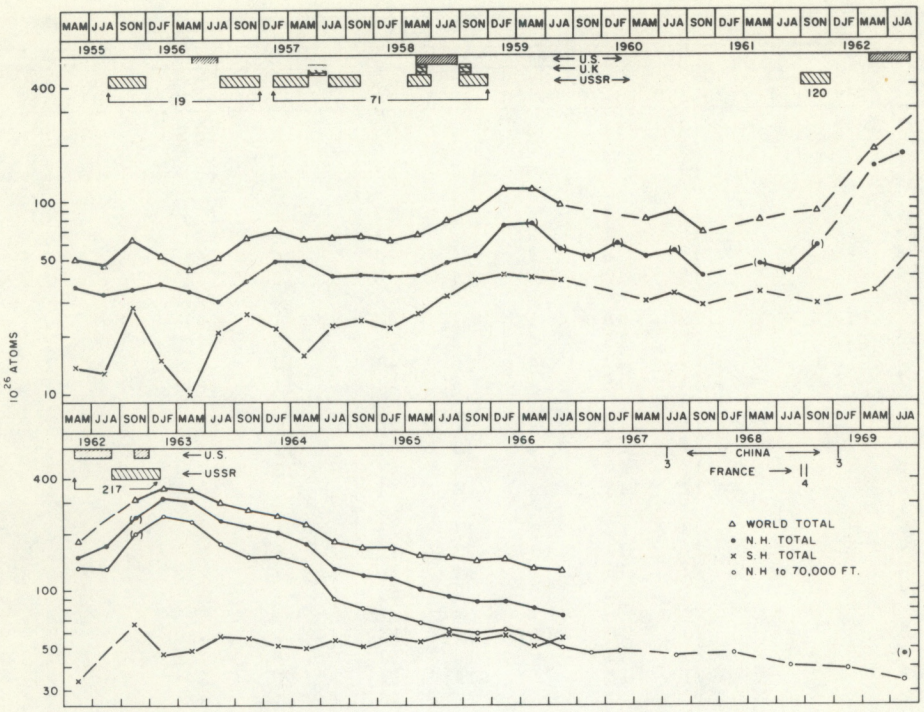

Figure 7.2. Stratospheric burden of excess C-14.

data exist in the Northern Hemisphere stratosphere to 70,000 ft through July 1969 to calculate the stratospheric burden to this altitude. This is shown in figure 7.2 for the period March 1962 to July 1969 and can be used as an indicator of the depletion rate of the stratosphere.

An improved high altitude molecular sieve sampler has been developed for the U.S. Atomic Energy Commission. Experimental flights in mid-1969 have been conducted at San Angelo, Texas, (31°N) from 70,000 to 120,000 ft (Ashenfelter et al., 1971). From September to November 1970 the molecular sieve sampler was flown successfully at six locations: Alaska (65°N), Iowa (42°N), Texas (31°N), Panama (9°N) and Australia (23°S and 34°S). Preliminary data from these flights were used to estimate the stratospheric burden in the Northern and Southern Hemispheres above 70,000 ft, shown in table 7.1 with brackets, (Telegadas, 1971).

The changes in the excess C-14 world stratospheric burden with time (shown in fig. 7.2) indicate that from 1955 to early 1959 the increase is caused by nuclear testing. From early 1959 to mid-1961 no large-yield atmospheric tests were conducted, and this is reflected by the decrease in the stratospheric burden. The intense 1961-1962 nuclear tests caused an increase in the stratospheric burden, reaching a peak in early 1963, about a factor of four higher than in mid-1961. From 1963 to July 1966, the last period with data throughout the stratosphere, a decrease in the stratospheric burden occurs since no high-yield atmospheric tests were conducted.

The high-yield tests between 1955 and 1962 occurred principally in the Northern Hemisphere. The changes in this portion of the stratosphere are similar to the world total, as seen in figure 7.2. The Southern Hemisphere stratospheric burdens, even though they are less reliable, show a gradual increase from 1955 to mid-1963 and then remain almost constant to mid-1966.

The June 17, 1967, Chinese nuclear test (40°N), about 3 megatons total yield, should have injected about 6×10^{26} C-14 atoms into the lower stratosphere to about 70,000 ft. The Northern Hemisphere stratospheric burden to 70,000 ft prior to this injection can be estimated from table 7.1 to be about 45×10^{26} excess C-14 atoms. The Chinese test should have increased the stratospheric burden by about 15 percent. It is not reflected in the July 1967 inventory, probably because the debris had little chance to spread latitudinally into the limited sampling network.

The excess C-14 stratospheric inventory prior to the December 28, 1968, Chinese nuclear test of about 3 megatons total yield was about a factor of 6 higher than the new input. Again this injection is not reflected in the February 1969 inventory calculations. Similarly, the 1968 high-yield French tests at 22°S are only partially reflected in the inventory because of the limited observational network.

7.2 Tropospheric Inventories

The tropospheric burdens for the Northern and Southern Hemispheres have been estimated from the seasonal distribution of excess C-14 presented by Telegadas (1971). In most cases the Northern Hemisphere had three locations where vertical profiles were collected, while the Southern Hemisphere had only one. It was assumed that Southern Hemisphere data were representative of the average tropospheric concentration for the entire hemisphere. The tropospheric burdens are given in table 7.2 with the Northern and Southern Hemisphere stratospheric burden repeated from table 7.1. The total world atmospheric burden (from surface to 100,000 ft) is given in the last column of table 7.2. The tropospheric burden is shown graphically in figure 7.3. A rapid rise in the burden is noted for both hemispheres following the 1958 U.S. and U.S.S.R nuclear tests. The burdens reach a maximum by mid-1959 and decrease thereafter with the burden in both hemispheres becoming about equal by mid-1960. The rapid rise in the tropospheric burden from the massive 1961-1962 nuclear tests is quite evident in figure 7.2. The Northern Hemispheric burden reaches a maximum in mid-1963, whereas the Southern Hemisphere reaches a maximum by mid-1965. By early 1966 the burden in both hemispheres is about equal.

7.3 Effective Residence Half-Times

The rate of decrease of the stratospheric and tropospheric burdens of excess C-14 in the years since the massive 1961-1962 nuclear tests can be estimated without significant interference from new injections. One can calculate the residence time of excess C-14 for the entire atmosphere which would provide a quantitative measure of the rate of exchange of atmospheric carbon dioxide with the ocean and biosphere "sink". The residence half-time is that time required for the reservoir

Table 7.2. Excess C-14 Inventory (atoms × 10^{26})

Quarter	Stratosphere			Troposphere		Atmosphere
	Northern Hemisphere	Southern Hemisphere	Total	Northern Hemisphere	Southern Hemisphere	Total
3/55- 5/55	36	(14)	50	--	--	--
6/55- 8/55	33	(13)	46	--	--	--
9/55-11/55	35	(28)	63	21	--	--
12/55- 2/56	37	(15)	52	9	--	--
3/56- 5/56	34	(10)	44	--	21	--
6/56- 8/56	30	(21)	51	8	11	70
9/56-11/56	38	(26)	64	13	6	83
12/56- 2/57	48	(22)	70	8	4	82
3/57- 5/57	48	(16)	64	8	4	76
6/57- 8/57	41	(23)	64	20	2	86
9/57-11/57	41	(24)	65	9	5	79
12/57- 2/58	40	(22)	62	12	8	82
3/58- 5/58	41	(26)	67	19	14	100
6/58- 8/58	47	(32)	79	25	21	125
9/58-11/58	51	39	90	29	28	147
12/58- 2/59	73	(41)	114	61	41	216
3/59- 5/59	(75)	(40)	115	59	--	--
6/59- 8/59	(56)	(39)	95	69	53	217
9/59-11/59	(51)	--	--	57	--	--
12/59- 2/60	(59)	--	--	--	--	--
3/60- 5/60	51	(30)	81	52	44	177
6/60- 8/60	(54)	(33)	87	46	45	178
9/60-11/60	40	(29)	69	44	45	158
12/60- 2/61	--	--	--	--	--	--
3/61- 5/61	(46)	(33)	79	56	54	189
6/61- 8/61	(43)	--	--	--	--	--
9/61-11/61	(58)	(29)	87	57	46	190
12/61- 2/62	--	--	--	--	--	--
3/62- 5/62	150	(34)	184	81	57	322
6/62- 8/62	171	--	--	85	--	--
9/62-11/62	(245)	(66)	311	98	72	481
12/62- 2/63	310	(46)	356	107	76	539
3/63- 5/63	300	(49)	349	179	84	612
6/63- 8/63	243	(58)	301	149	86	536
9/63-11/63	215	(57)	272	147	97	516
12/63- 2/64	203	(52)	255	144	105	504
3/64- 5/64	176	(49)	225	151	112	488
6/64- 8/64	128	(55)	183	148	110	441
9/64-11/64	119	(51)	170	133	116	419
12/64- 2/65	113	(57)	170	133	116	419
3/65- 5/65	101	(55)	156	139	118	413
6/65- 8/65	92	(59)	151	147	128	426
9/65-11/65	88	(56)	144	142	128	414
12/65- 2/66	88	(58)	146	130	126	402
3/66- 5/66	79	(52)	131	132	126	389
6/66- 8/66	73	(55)	128	128	126	382
9/66-11/66	--	--	--	--	--	--
1/67	--	--	--	123	123	--
7/67	--	--	--	117	114	--
1/68	--	--	--	119	114	--
6/68	--	--	--	106	107	--
2/69	--	--	--	107	105	--
7/69	45	(41)	86	102	100	288

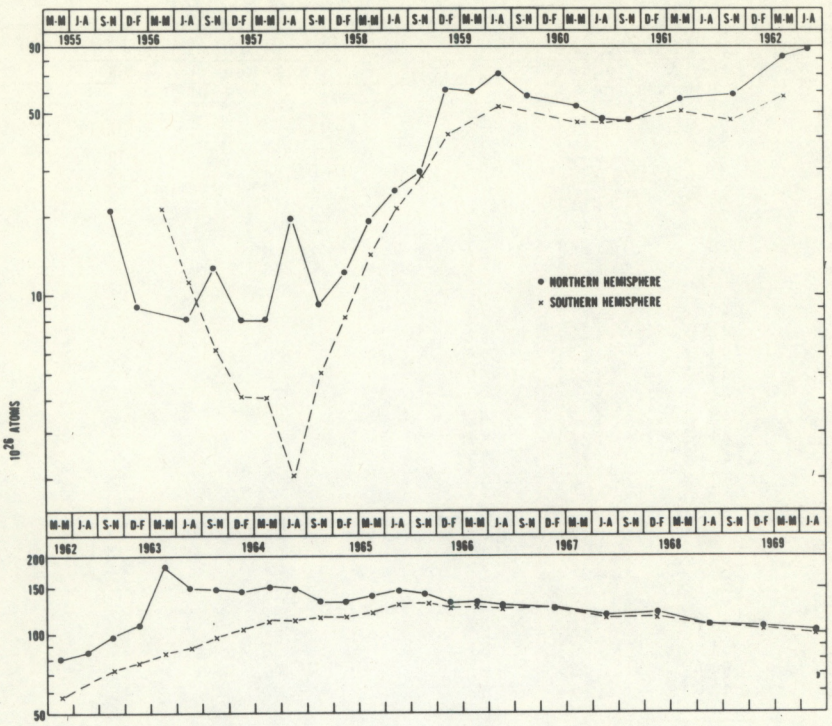

Figure 7.3. Tropospheric burden of excess C-14.

containing an initial amount of material to decrease to one-half that amount. The assumption inherent in this definition is that the fractional removal is constant from a uniformly mixed reservoir such that mixing preserves uniformity of concentration in the reservoir. Unfortunately, the excess C-14 in the atmosphere is not well mixed and the ocean-biosphere compartment not only acts as a sink but also as a source region. We therefore are using the term *effective* residence half-time as the time for a reservoir to reduce to half its content without regard to transfers from other reservoirs.

The effective residence half-time is shown graphically for the total stratosphere and total atmosphere in figure 7.4 and is summarized in table 7.3. For the entire stratosphere it can be seen that, for the period 1963 to mid-1966 (when

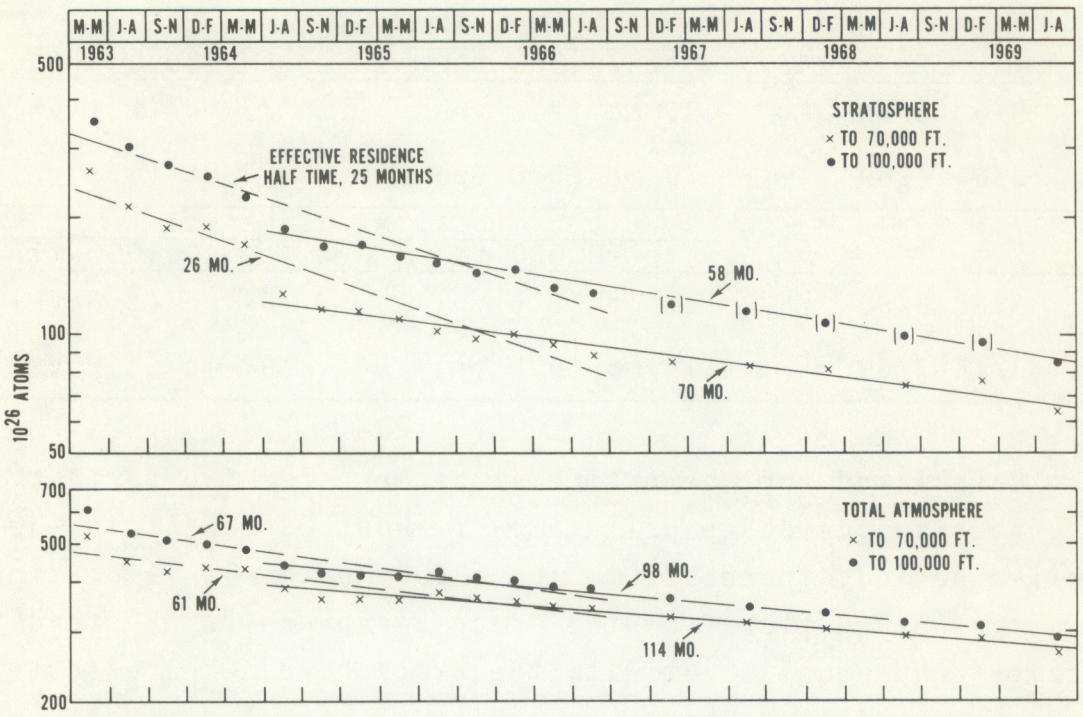

Figure 7.4. The effective residence half-time of excess C-14 for the total stratosphere and total atmosphere.

the data were plentiful), the effective residence half-time (line of best fit) for the stratospheric burden to 70,000 and to 100,000 ft is the same — about 25 months. It is quite obvious from figure 7.4 that the effective residence half-time for the stratosphere starting in mid-1964 is longer. The stratosphere to 70,000 ft, where the inventory is considered more reliable than that to 100,000 ft, indicates an effective residence half-time of about 70 months. This shift in the effective residence half-time is probably brought about by the fact that the stratosphere (source region) and the troposphere (sink region) tend toward equilibrium and the return flow from the troposphere into the stratosphere becomes effective in lengthening the residence half-time. In the lower portion of figure 7.4, the effective residence half-time has

Table 7.3. Effective Residence Half-Time

	World Stratosphere	
	to 70,000 ft	to 100,000 ft
3/63-8/66	26 mo (2.2 yr)	25 mo (2.1 yr)
6/64-7/69	70 mo (5.8 yr)	58 mo (4.8 yr)
	Total Atmosphere	
	to 70,000 ft	to 100,000 ft
3/63-8/66	61 mo (5.6 yr)	67 mo (5.6 yr)
6/64-7/69	114 mo (9.5 yr)	98 mo (8.2 yr)

been calculated for the entire atmosphere for two periods. An effective residence half-time of about 65 months in the earlier periods increases to about 100 months at later times when the return flow from the ocean-biosphere "sink" tends to establish an equilibrium with the atmosphere. The effective residence half-times given in table 7.3, for the stratosphere and atmosphere are upper limits of the true residence half-times.

The excess C-14 data are being used to develop a simple multireservoir exchange model for carbon dioxide. The reservoirs are: stratosphere, troposphere, mixed layer of the ocean, deep ocean, short-term land biosphere, long-term land biosphere, and marine biosphere. Estimates of exchange coefficients between many of the reservoirs are available in the scientific literature; however, estimates of exchange coefficients for CO_2 transfer between atmospheric compartments and between the atmosphere and the ocean are uncertain. CO_2 molecules tagged with C-14 will provide substantially better estimates of these latter exchange rates. The model will be used to estimate past atmospheric CO_2 levels and to predict future levels based on known or estimated fossil fuel consumption rates.

7.4 References

Ashenfelter, T. E., J. Gray, Jr., M. Svendsen and K. Telegadas (1972), Measurements of stratospheric C-14 with an improved molecular sieve sampler, J. Geophys. Res., *77*, No. 3, pp. 412-419.

Environmental Science Services Administration (1966), Carbon-14 measurements in the atmosphere, HASL-166, January 1966.

Environmental Science Services Administration (1967), Carbon-14 measurements in the atmosphere, HASL-174, January 1967.

Environmental Science Services Administration (1969), Carbon-14 measurements in the atmosphere, HASL-214, October 1969.

Hagemann, F., J. Gray, Jr., and L. Machta (1965), Carbon-14 measurements in the atmosphere 1953 to 1964, HASL-159, April 1965.

Krey, P. W., M. Kleinman and B. Krajewski (1969), Strontium-90 stratospheric inventories, 1967-1968, HASL-210, July 1969.

Machta, L., R. J. List and K. Telegadas (1963), Meteorology of fallout from 1961-1962 nuclear tests, Congress of the United States Hearing before Subcommittee in Research, Development and Radiation of the Joint Committee of Atomic Energy, 88th Congress, 46-61, June 1963.

National Oceanic and Atmospheric Administration (1971), Carbon-14 measurements in the atmosphere, HASL-242, April 1971.

Telegadas, K. (1971), The seasonal atmospheric distribution and inventories of excess Carbon-14 from March 1955 to July 1969, HASL-243, July 1971.

U.S. Atomic Energy Commission (1968), Note to editors and correspondents, No. L-294, 1968, USAEC, Washington, D.C., 20545.

U.S. Weather Bureau (1964), Announced nuclear detonations, 1945-1962, HASL-142, January 1964.